Factor Graph-Based Equalization for Two-Way Relaying With General Multi-Carrier Transmissions

Matthias Woltering, *Student Member, IEEE*, Dirk Wübben, *Senior Member, IEEE*, and Armin Dekorsy, *Member, IEEE*

***Abstract*— Multi-carrier transmission schemes with general non-orthogonal waveforms provide a flexible time-frequency resource allocation and are bandwidth efficient. However, the interference inherently introduced by the non-orthogonal waveforms always requires a higher order equalizer at the receiver. Depending on the localization properties of the applied waveform, the structure and the complexity of this equalizer is adapted to consider channel influences, like carrier frequency and timing offsets. Especially for two-phase two-way relaying channels (TWRCs), where two users simultaneously transmit data on the same resources, a robust transmission scheme in presence of practical constraints such as asynchronicity is of utmost importance. This paper focuses on the utilization of general multi-carrier transmission schemes applied to TWRCs and the utilization of factor graph-based equalizers (FGEs) at the relay in order to mitigate the impacts of the physical channels, offsets, and the non-orthogonal waveforms. In combination with the subsequent physical-layer network coding detection/decoding scheme, this combination allows for a flexible design of the waveforms and the FGE to meet the complexity-performance trade-off at the relay. As demonstrated by numerical evaluation results, the proposed multi-carrier scheme with well-localized waveforms utilizing FGEs outperforms orthogonal frequency division multiplexing in TWRC for a wide range of practical impacts.**

***Index Terms*— Multi-carrier, general waveform, two-way relaying channels, factor graph-based equalizer.**

I. Introduction

USER cooperation in wireless communications enhances system performance and reliability and extends coverage. Specifically, in TWRCs in which a number of users wants to exchange information via an assisting relay, the communication overhead can be reduced by bidirectional relaying in two phases [2]–[4]. Within this article, we consider TWRCs and a pair of users with no direct link transmitting simultaneously to the relay in the multiple access (MA) phase. The resulting multi-user interference (MUI) at the relay can be exploited by interpreting the superposition of the user messages by means of physical-layer network coding (PLNC). The relay has the task of estimating the bit-level eXclusive OR (XOR) combination of the underlying information bits and broadcasts this PLNC-based relay message to the users. As the users are aware of their own information, they can extract the useful information from relay message. The most critical part of such a communication system is the estimation of the relay message based on the superimposed user messages in the MA phase. Several PLNC approaches, which combines *detection* and *decoding* such as separate channel decoding (SCD) [2], joint channel decoding and physical-layer network coding (JCNC) [2], [3] and generalized-JCNC (G-JCNC) [5] have been proposed in the literature for estimating the relay message in single-carrier (SC) transmissions over frequency flat channels.

For frequency-selective TWRCs and SC transmission, a linear equalization approach for mitigating the introduced intersymbol interference (ISI) while exploiting the MUI has been proposed in [6]. A frequently applied alternative to reduce the receiver complexity for frequency-selective channels is the filter bank multi-carrier (FBMC) transmission scheme cyclic prefix (CP)-orthogonal frequency-division multiplexing (CP-OFDM) In synchronous systems, it allows for simple 1-tap equalization at a reduced bandwidth efficiency by the expense of a CP. Consequently, the utilization of CP-OFDM for TWRC has been analyzed intensively (*e.g.*, [7], [8]). However, as indicated by theoretical investigations [9] and demonstrated by corresponding hardware implementations [10], [11] this CP-OFDM-TWRC system is very sensitive to node asynchronicity like carrier frequency offsets (CFOs) or timing offsets (TOs) resulting in ISI and intercarrier interference (ICI). For point-to-point (P2P) transmissions, these impacts could be estimated and pre-compensated at the receiver such that a simple 1-tap frequency domain equalizer is still sufficient. In contrast, in TWRC these impacts cannot be resolved individually at the relay, but only an average compensation is possible and a simple 1-tap equalizer would lead to severe performance degradation [10]–[12].

Apart from cooperative communication, the need for a higher number of devices motivated the discussion of new waveform candidates for the 5$^{\text{th}}$ generation (5G) mobile communication system [13], [14]. In particular, these systems should offer better spectral shapes, flexible time-frequency (TF) resource allocations [15], and a higher robustness against practical impairments (*e.g.*, TO, CFO). To improve the robustness for P2P transmissions over doubly-dispersive channels,

Manuscript received February 13, 2017; revised June 23, 2017 and September 22, 2017; accepted November 12, 2017. Date of publication November 28, 2017; date of current version February 9, 2018. This work was presented at the 10th International ITG Workshop on Smart Antennas in Munich, Germany, in 2016 [1]. The associate editor coordinating the review of this paper and approving it for publication was T. M. Duman. *(Corresponding author: Matthias Woltering.)*

The authors are with the Department of Communications Engineering, University of Bremen, 28359 Bremen, Germany (e-mail: woltering@ant.uni-bremen.de).

Color versions of one or more of the figures in this paper are available online at http://ieeexplore.ieee.org.

Digital Object Identifier 10.1109/TWC.2017.2776941

the use of FBMC transmission schemes applying general non-orthogonal *well-localized* waveforms with concentrated energy in frequency and time domain was proposed in [16]. Despite their non-orthogonal nature, the inherently introduced interference terms change only marginally under TO and CFO in contrast to CP-OFDM systems employing rectangular waveforms. Thus, the equalizer structure at the destination remains almost unchanged under more severe channel conditions.

Due to their robust characteristics under offsets, the utilization of FBMC transmission schemes with well-localized waveforms for TWRC was proposed by the authors in [17] and a linear equalizer based on [6] has been derived to deal with the resulting interference. In particular, the good localization property of the Gaussian waveform offers a reduction in the window size of the linear equalizer [18]. Further performance improvements have been demonstrated in [19] by the application of a soft interference cancellation algorithm. These results were summarized and extended by an analysis *w.r.t.* changing TF grid spacings in [20] establishing a framework for jointly designing the waveform and the equalizer.

Over the past decades, factor graphs (FGs) and the underlying message passing algorithm have been used intensively for a variety of applications like error correction coding, Kalman filtering, and iterative detection [21]–[23]. For SC transmission over time-invariant channels, factor graph-based equalizers (FGEs) have been discussed in [24]–[28], and extended for time-variant channels in [29]. Further extensions for multiple input multiple output (MIMO) antenna systems [30]–[32], single input single output (SISO)-orthogonal frequency division multiplexing (OFDM) with time-variant channels [33] and MIMO-OFDM [34], [35] indicated the excellent performance of FG-based detection/equalization similar to the corresponding optimal algorithms (even if the FGs have a small girth due to the present ISI or ICI [31]). First applications of an FGE for SC-TWRC have been proposed for the time and phase asynchronous case in [36] and for CP-OFDM modulated TWRC with time-variant (doubly-dispersive) channels in [37], [38].

The combination of general robust waveforms for FBMC transmissions and the adaptive design of the FGE for a P2P transmission was first proposed by the authors in [1]. It offers a joint design of the general FBMC transmission and the equalizer leading to improved performance for a broad range of offsets. As the complexity of the message passing algorithm is mainly controlled by the number of connections in the FG, the performance-complexity trade-off can be regulated by adjusting the parameters of the general (*i.e.*, non-orthogonal) waveform. Thus, the FGE can iteratively deal with the "well-localized" influences of the waveform in the equalization step. In addition to P2P transmission, the authors have also presented first ideas and results for the joint application of general FBMC and FGE for TWRC in [1]. A detailed discussion of the TWRC-related aspects with the following main contributions is provided:

- The focus of this work is the design of an FGE for PLNC schemes interacting with FBMC transmission schemes applying general waveforms within two-phase TWRC. This design offers an adaptive and flexible framework which gets elaborated especially under channel impairments.
- We provide a comprehensive description of the overall system model as an FG including the equalizer, the demodulator, and the decoder.
- An interference analysis *w.r.t.* timing and frequency offsets in terms of the interference power is provided and the FBMC system with quadrature amplitude modulation (QAM) or offset-QAM (OQAM) symbol mapping is compared to the state-of-the-art CP-OFDM.

This paper is organized as follows: Due to the multi-dimensional nature of the problem of transmission and detection, we start with a brief overview of the two-phase TWRC communication and the PLNC approaches used in this work in Section II. Section III introduces the system model of the MA phase in matrix description and discusses the mapping of the information bits to the physical resources by applying general FBMC schemes. Here, we first focus on the general properties of the FBMC schemes within a single P2P transmission *w.r.t.* interference terms introduced by TO and CFO. A deeper interference analysis by the extension to TWRCs is provided in Section IV. It is shown that for a wide range of offsets most of the interference terms are concentrated on the neighboring sub-carriers and time-symbols for general non-orthogonal waveforms. Thus, compared to CP-OFDM, only a few number of interference terms have to be considered to collect the useful power at the destination. As discussed in Section V, the FGE needs to be adapted for the chosen PLNC scheme. To this end, we introduce the message passing procedure, outline the calculation of the messages, and discuss the required modifications to meet the implications of the PLNC detection/decoding. Finally, the performance analysis in terms of frame error rates (FERs) at the relay is discussed in Section VI, before Section VII concludes the article.[1]

II. TWRC Overview

We consider a two-phase TWRC, where two users A and B want to exchange data with each other by the help of an assisting relay R located between both entities. Within the first phase (MA phase), both users $\mathsf{u} \in \{\mathsf{A}, \mathsf{B}\}$ encode with a linear forward error correction (FEC) encoder $\mathcal{C}$ and map their information messages $\mathbf{b}^{\mathsf{u}}$ to the physical resources $x^{\mathsf{u}}(t)$ and transmit simultaneously to the relay, where t denotes the time. At the relay, the noisy superposition $y^{\mathsf{R}}(t)$ of both transmit signals convolved with their time-variant multi-path channels $w^{\mathsf{u}}(\tau, t)$ is achieved

$$y^{\mathsf{R}}(t) = w^{\mathsf{A}}(\tau, t) * x^{\mathsf{A}}(t) + w^{\mathsf{B}}(\tau, t) * x^{\mathsf{B}}(t) + n(t), \quad (1)$$

in which $n(t)$ is the additive white Gaussian noise (AWGN) and τ denotes the delay. This transmission is also illustrated in Fig. 1 as TWRC block.

[1]The following notations are applied in this work: Scalars, column vectors, and matrices are denoted by small characters a, small bold characters $\mathbf{a}$, and capital bold characters $\mathbf{A}$, respectively. The real and imaginary part operators are given by $\mathrm{Re}\{\cdot\}$ and $\mathrm{Im}\{\cdot\}$. A probability density function (PDF) is given by $\mathrm{p}(\cdot)$ and a probability mass function (PMF) by $\Pr\{\cdot\}$. $\mathbb{F}_n$ determines a Galois Field of order n. A hard decision of a variable b is denoted by $\hat{b}$.

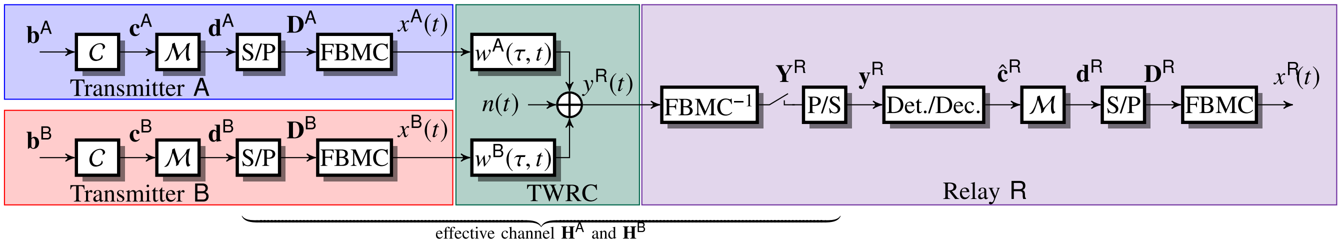

Fig. 1. System model of MA phase, TWRC and relay process chain to generate the relay message $x^{\mathsf{R}}(t)$.

The task at the relay is the detection of a common relay message, which is broadcast (BC) in the second phase to both users. The received relay signal (1) can be seen as a PLNC signal [2], [3] and the relay message $\mathbf{b}^{\mathsf{R}}$ is generated by the XOR combination of the individual messages $\mathbf{b}^{\mathsf{R}} = \mathbf{b}^{\mathsf{A}} \oplus \mathbf{b}^{\mathsf{B}}$. Other network coding combinations are possible as well and discussed in [39]. The relay message $\mathbf{b}^{\mathsf{R}}$ is mapped to the signal $x^{\mathsf{R}}(t)$ and broadcast to both users. The user A estimates $\hat{\mathbf{b}}^{\mathsf{R}}$ and is able to extract the signal from user B by performing self-interference cancellation $\hat{\mathbf{b}}^{\mathsf{B}} = \hat{\mathbf{b}}^{\mathsf{R}} \oplus \mathbf{b}^{\mathsf{A}}$. Similarly, user B extracts the useful information by $\hat{\mathbf{b}}^{\mathsf{A}} = \hat{\mathbf{b}}^{\mathsf{R}} \oplus \mathbf{b}^{\mathsf{B}}$ by its estimate of the relay message $\hat{\mathbf{b}}^{\mathsf{R}}$. The major challenge is the generation of the relay message $\mathbf{b}^{\mathsf{R}}$ based on the superposition (1) in the MA phase at the relay. Contrarily, the transmission in the BC phase can be seen as two P2P transmissions from the relay to each user. Consequently, the analysis in this paper is restricted to the MA phase utilizing alternatively one of the three PLNC approaches:

- In *separate channel decoding* (SCD) each user message $\hat{\mathbf{b}}^{\mathsf{u}}$ is estimated separately at the relay, treating the other user as interference [5]. The relay message is achieved by performing the XOR combination of these estimates afterward by $\mathbf{b}^{\mathsf{R}} = \hat{\mathbf{b}}^{\mathsf{A}} \oplus \hat{\mathbf{b}}^{\mathsf{B}}$.
- In contrast, *joint channel decoding and physical-layer network coding* (JCNC) directly estimates the relay message $\mathbf{b}^{\mathsf{R}}$ by exploiting the linearity of the applied channel code $\mathcal{C}$ [2].
- Furthermore, *generalized-JCNC* (G-JCNC) is an extension of JCNC interpreting the messages of both users as a joint information message tuple $\mathbf{b}^{\mathsf{AB}}$ and uses a non-binary decoder [5], [7]. This scheme offers the best performance by the utilization of the fully available underlying information. The message for the BC phase is generated by simply mapping the estimated tuple $\hat{\mathbf{b}}^{\mathsf{AB}}$ to the relay message $\mathbf{b}^{\mathsf{R}}$.

Under mild channel conditions like time-invariant channels with short delay spread, these detection/decoding schemes exhibit good performance in combination with CP-OFDM [10], [11], [40], [41]. However, channels with large TOs or time-variant channels yield degraded performance at the relay due to the huge amount of interference which cannot be compensated individually at the relay. General FBMC schemes applying non-orthogonal waveforms with good localization properties in time and frequency domain are able to offer better performance under severe channel conditions in TWRC [20]. Thus, we introduce the general system model of different FBMC schemes and discuss the impact of TO and CFO in the MA phase on a TWRC, subsequently. Afterward, we discuss the details of the combination of PLNC detection and FGEs.

III. Multi-Carrier Transmission in Multiple Access Phase

A. System Model

Fig. 1 shows the detailed system model for the FBMC transmission of two users to the relay in the MA phase. The users and the relay are equipped with one antenna and all nodes are restricted to the half-duplex constraint. Each user $\mathsf{u} \in \{\mathsf{A}, \mathsf{B}\}$ encodes its binary information sequence $\mathbf{b}^{\mathsf{u}} \in \mathbb{F}_2^{N_b}$ of length N_b with a linear encoding scheme to the codeword $\mathbf{c}^{\mathsf{u}} = \mathcal{C}(\mathbf{b}^{\mathsf{u}}) \in \mathbb{F}_2^{N_c}$ of length N_c. In this work, we apply low-density parity check (LDPC) codes as they show a good performance and can be efficiently decoded based on FGs. After modulation with an M-QAM mapper $\mathcal{M}$ (or M-OQAM, which will be introduced and discussed in Section III-C) and serial-to-parallel (S/P) conversion, the symbol matrix $\mathbf{D}^{\mathsf{u}} \in \mathbb{C}^{N_{\mathrm{SC}} \times N_{\mathrm{TS}}}$ is generated, where N_{SC} is the number of sub-carriers and N_{TS} is the number of time symbols used in one frame transmission. The FBMC block maps the symbol matrix $\mathbf{D}^{\mathsf{u}}$ to the physical transmit signal $x^{\mathsf{u}}(t)$. To this end, each element $d_{k,\ell}^{\mathsf{u}}$ of $\mathbf{D}^{\mathsf{u}}$ is shifted to a point in the TF grid by a bank of transmitting filters

$$g_{k,\ell}^{\mathrm{Tx}}(t) = g(t - \ell T_0) \mathrm{e}^{j2\pi(kF_0)t}, \tag{2}$$

in which the prototype waveform filter $g(t)$ is shifted by multiples of the symbol spacing T_0 and the sub-carrier spacing F_0 to the corresponding time-frequency (TF) point (k, ℓ) resulting in a rectangular grid as illustrated in Fig. 2a [42].

After transmitting the signals $x^{\mathsf{u}}(t)$ over the analog wireless physical channels $w^{\mathsf{u}}(\tau, t)$ to the relay, a bank of matched filters $g^{\mathrm{Rx}}(t) = g^{\mathrm{Tx}*}(-t)$ is applied to the received relay signal (1) and sampled such that a discrete receive signal matrix $\mathbf{Y}^{\mathsf{R}} \in \mathbb{C}^{N_{\mathrm{SC}} \times N_{\mathrm{TS}}}$ is obtained. After parallel-to-serial (P/S) conversion, the overall transmission is described by the linear superposition of both users in matrix notation

$$\mathbf{y}^{\mathsf{R}} = \mathbf{H}^{\mathsf{A}} \mathbf{d}^{\mathsf{A}} + \mathbf{H}^{\mathsf{B}} \mathbf{d}^{\mathsf{B}} + \tilde{\mathbf{n}}^{\mathsf{R}}, \tag{3}$$

where $\tilde{\mathbf{n}}^{\mathsf{R}} \in \mathbb{C}^{N_{\mathrm{SC}} N_{\mathrm{TS}} \times 1}$ contains noise samples modeled by $\mathcal{N}_{\mathcal{C}}\left\{0, \sigma_{\mathrm{n}}^2\right\}$. The P/S conversion corresponds to stacking the columns of matrix $\mathbf{Y}^{\mathsf{R}}$ into a vector $\mathbf{y}^{\mathsf{R}} \in \mathbb{C}^{N_{\mathrm{SC}} N_{\mathrm{TS}} \times 1}$ and is described by the vectorization operator $\mathbf{y}^{\mathsf{R}} = \mathrm{vec}\left\{\mathbf{Y}^{\mathsf{R}}\right\}$.

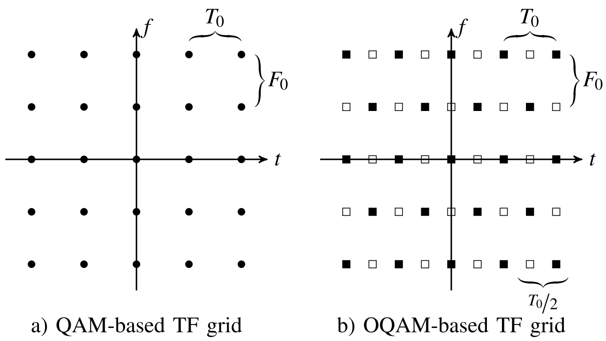

Fig. 2. TF grids a) QAM-based: Rectangular TF grid with sub-carrier spacing kF_0 and time spacing ℓT_0 with complex symbols denoted by filled circles, b) OQAM-based: Two hexagonal TF grids with real data denoted by black filled squares and purely imaginary data by white filled squares [43].

Similarly, the data symbol vectors $\mathbf{d}^{\mathsf{u}} = \operatorname{vec}\{\mathbf{D}^{\mathsf{u}}\}$ are generated. The *effective channel matrix* $\mathbf{H}^{\mathsf{u}} \in \mathbb{C}^{N_{\mathrm{SC}}N_{\mathrm{TS}} \times N_{\mathrm{SC}}N_{\mathrm{TS}}}$ per user $\mathsf{u} \in \{\mathsf{A}, \mathsf{B}\}$ depends on the physical channel $w^{\mathsf{u}}(\tau, t)$ and the used FBMC transmission scheme. For further details about different FBMC schemes, the reader is referred to the survey [42]. In this work, we concentrate on general FBMC schemes which are mainly classified by the choice of the Tx/Rx waveforms, the mapping scheme $\mathcal{M}$, and the density δ_{TF} of the symbol-spacing in time and frequency (the *TF grid density*). The density δ_{TF} of a rectangular grid is given by $\delta_{\mathrm{TF}} = 1/(F_0 T_0)$. Three different cases are known: 1) *oversampled*: $\delta_{\mathrm{TF}} > 1$, this TF grid is too dense, such that no orthogonal transmission is possible, 2) *critical sampled*: $\delta_{\mathrm{TF}} = 1$, where an orthogonal system can only be achieved with filters of infinite shape (ill-conditioned), *e.g.* the rectangular waveform in time domain with sinc shape in frequency domain, and 3) *undersampled*: $\delta_{\mathrm{TF}} < 1$, an orthogonal transmission is possible with well-localized filters [42]. For the Tx/Rx filters, we concentrate on the time-limited *rectangular waveform*, the frequency-limited *half-cosine*, and the *Gaussian* waveform. The latter one is not limited, but "well-localized", *i.e.*, with concentrated energy in time and frequency domain. In this article, we focus on seven different QAM and OQAM-based FBMC transmission schemes with critical and under-sampled TF grids and compare non-orthogonal with orthogonal transmission schemes, which are listed in Tab. I and get introduced in the following subsections.

The elements $h^{\mathsf{u}}_{r,s}$ of the effective channel matrix $\mathbf{H}^{\mathsf{u}}$ are given by (4), as shown at the bottom of this page, with parameters given in Tab. I and the system-dependent TF grid spacing parameter T' and symbol phase parameter ϕ. Please note that to simplify the notation, we introduce sending index $s = k + \ell N_{\mathrm{SC}}$ and the receiving index $r = k' + \ell' N_{\mathrm{SC}}$ for the matrix elements $h^{\mathsf{u}}_{r,s}$, where (k, ℓ) specifies a distinct point in the TF grid at the transmit (Tx) side and (k', ℓ') are the

TABLE I
FBMC TRANSMISSION SCHEMES

	QAM-based FBMC	OQAM-based FBMC
	$T' = T_0 = T + T_{\mathrm{G}}$ $\phi = 0$	$T' = T_0/2 = T/2$ $\phi = \frac{\pi}{2}(k' - k + \ell' - \ell)$
rectangular	OFDM, $T_{\mathrm{G}} = 0$	OQAM/OFDM
rect. with CP	CP-OFDM, $T_{\mathrm{G}} \neq 0$	–
Gaussian	QAM/FBMC, $T_{\mathrm{G}} = 0$	OQAM/FBMC
half-cosine	QAM/FBMC, $T_{\mathrm{G}} = 0$	OQAM/FBMC

TF grid points at the relay. Hence, the effective channel coefficient $h^{\mathsf{u}}_{r,s}$ reflects the crosstalk from symbol $d^{\mathsf{u}}_s = d^{\mathsf{u}}_{k,\ell}$ onto observation $y^{\mathsf{R}}_r = y^{\mathsf{R}}_{k',\ell'}$. It is worth noting that the effective channel coefficients $h^{\mathsf{u}}_{r,s}$ depend on the delay-Doppler function $W^{\mathsf{u}}(\tau, \nu)$, which is given by the Fourier transform *w.r.t.* time t of the wireless channel $w^{\mathsf{u}}(\tau, t)$. Here, ν denotes the Doppler domain. Subsequently, we distinguish between constant shifts like TO $\Delta\tau$ and CFO $\Delta\nu$ and variable shifts like delay spread τ and Doppler spread ν specified by the corresponding PDFs. Furthermore, the coefficients $h^{\mathsf{u}}_{r,s}$ depend on the cross-ambiguity function

$$A_{g^{\mathrm{Tx}}, g^{\mathrm{Rx}}}(\tau, \nu) = \int_{-\infty}^{\infty} g^{\mathrm{Tx}}\Big(t - \frac{\tau}{2}\Big)\, g^{\mathrm{Rx}*}\Big(t + \frac{\tau}{2}\Big)\, e^{-j2\pi\nu}\mathrm{d}t, \quad (5)$$

describing the properties of the used Tx/Rx filters [17], [44]. The ambiguity function describes the behavior of a waveform for specific time shifts τ and frequency shifts ν, which occurs in transmissions over doubly-dispersive channels. It can be interpreted as the instantaneous Fourier transform of the convolution of the Tx and the Rx filters.

We rewrite the received signal (3) in scalar form per received symbol y^{R}_r into the sum of three parts

$$y^{\mathsf{R}}_r = \underbrace{h^{\mathsf{A}}_{r,r} d^{\mathsf{A}}_r + h^{\mathsf{B}}_{r,r} d^{\mathsf{B}}_r}_{\text{① PLNC signal}} + \underbrace{\sum_{s \neq r} \Big(h^{\mathsf{A}}_{r,s} d^{\mathsf{A}}_s + h^{\mathsf{B}}_{r,s} d^{\mathsf{B}}_s\Big)}_{\text{② mutual interference}} + \underbrace{\tilde{n}^{\mathsf{R}}_r}_{\text{③ noise}}. \quad (6)$$

These three parts contain the desired superposition ① called PLNC signal, the mutual interference ② depending on the channel and the chosen FBMC scheme, and the noise term ③.

Subsequently, we present the FBMC schemes and provide a brief analysis of the interference on one P2P link. The interference analysis for the considered TWRC is discussed in Section IV.

B. QAM-Based Multi-Carrier Schemes

In this subsection, we introduce the QAM-based multi-carrier schemes. We start with the well-known orthogonal

$$h^{\mathsf{u}}_{r,s} = \iint \underbrace{W^{\mathsf{u}}(\tau, \nu)}_{\text{delay-Doppler function}} \; e^{-2j\pi(kF_0\tau + (F_0(k'-k)-\nu)(\frac{1}{2}((\ell'+\ell)T'+\tau)))} \cdot \underbrace{A^*\big(T'\big(\ell - \ell'\big) + \tau,\, F_0\big(k - k'\big) + \nu\big)\, e^{j\phi}}_{\text{Tx/Rx waveforms}} \mathrm{d}\nu\mathrm{d}\tau \quad (4)$$

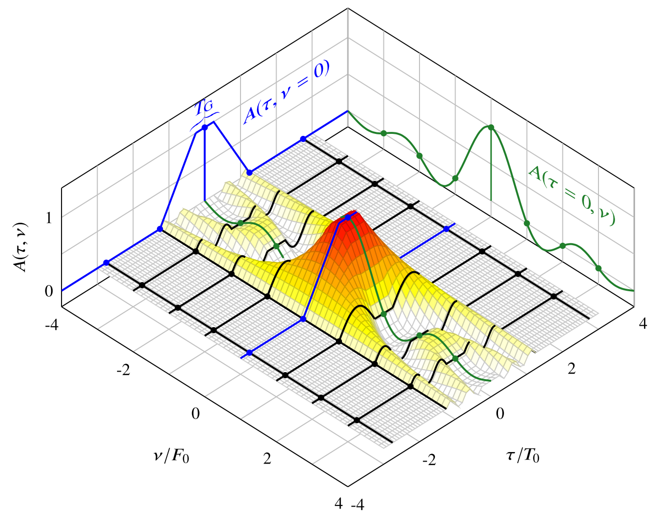

Fig. 3. Ambiguity function for rectangular Tx/Rx filters by additionally implementing a guard interval of length $T_G = 0.2T$ at the Tx side. This waveform is applied in CP-OFDM. The projections of $A(\tau = 0, \nu)$ at the time shift τ-plane and $A(\tau, \nu = 0)$ at the frequency shift ν-plane are shown, respectively.

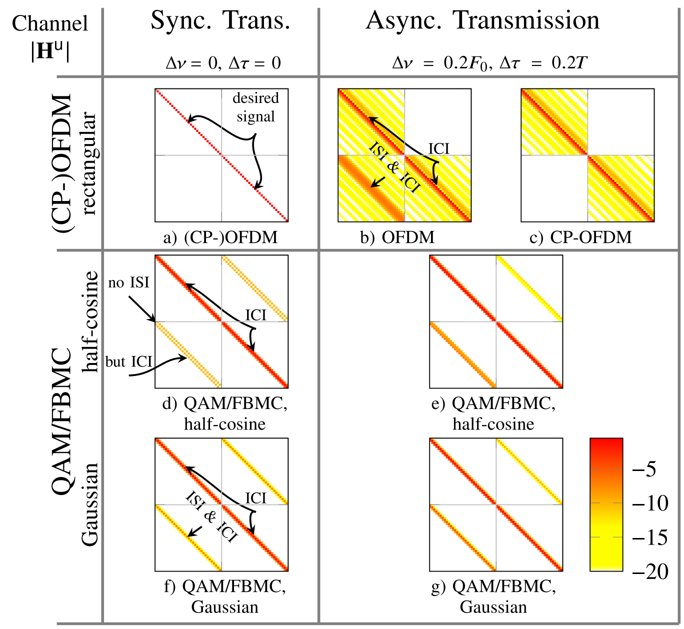

Fig. 4. Illustration of the amplitudes of the effective channel matrix with a) OFDM / CP-OFDM w/o offsets ($\Delta\nu = 0, \Delta\tau = 0$), b) OFDM w/ offsets ($\Delta\nu = 0.2F_0, \Delta\tau = 0.2T$), and c) CP-OFDM w/ offsets. The amplitudes of QAM/FBMC are depicted for the Gaussian waveform w/o offsets in d), and with offsets in e), and for the half-cosine waveform in w/o offsets in f), and w/ offsets in g). Only the first 64x64 elements are shown.

CP-OFDM applying the rectangular waveform before we introduce the non-orthogonal counterpart, *i.e.* QAM/FBMC, applying waveforms with a better spectral shape.

1) Orthogonal Transmission: The well-known OFDM is a special case of QAM-based FBMC applying the time-limited rectangular waveform

$$g(t) = \begin{cases} 1/\sqrt{T} & |t| \leq \dfrac{T}{2} + \dfrac{T_G}{2} \\ 0 & \text{else,} \end{cases} \tag{7}$$

as Tx filter with core symbol duration T and guard interval length T_G. In frequency domain, this Tx filter shows an infinite shape with $\mathrm{sinc}(f) = \sin(f)/f$, where f denotes the frequency. An orthogonal transmission is only achieved by placing the neighboring sub-carriers onto the zero-crossings of the sinc function, which are multiples of the reciprocal value of the symbol duration $F_0 = 1/T$. OFDM with a density $\delta_{TF} = 1$ is achieved for the special case of a guard interval length $T_G = 0$. However, in order to reduce the impact of multi-path fading $T_G > 0$ is required. With the common implementation as cyclic prefix (CP), the well-known CP-OFDM is realized. Please note that the application of a CP expands the TF grid spacing $T' = T_0 = T + T_G$ by the guard interval length T_G and leads to a reduced density $\delta_{TF} = \frac{T}{T+T_G} < 1$ with reduced spectral efficiency. One may note that $T_G = 0$ is used for the receive (Rx) filter $g^{Rx}(t)$. The ambiguity function of the rectangular Tx/Rx filters (7) with $T_G = 0.2T$ is shown in Fig. 3. The projection of a cut of the ambiguity function $A(\tau = 0, \nu)$ is drawn at the frequency shift ν-plane. This can be interpreted as the Fourier transform of the Tx/Rx filters and exhibits the sinc(ν) shape typical for rectangular filters. Cutting the ambiguity function $A(\tau, \nu = 0)$ equals the convolution of the Tx and Rx filters in time domain.

In Fig. 3 the multiples of the sub-carrier and symbol spacing are depicted by lines on the surface of the ambiguity function. The sampling points (k, ℓ) of the TF grid matches to the corresponding crossing points. If the orthogonality condition

$$A(kF_0, \ell(T + T_G) + \tau) = \begin{cases} 1 & k = 0, \ell = 0, |\tau| \leq \dfrac{T_G}{2} \\ 0 & \text{else} \end{cases} \tag{8}$$

is fulfilled, the Tx/Rx filters allow an orthogonal transmission, and thus, no self-interference terms are present on the neighboring TF grid points. Without a guard interval ($T_G = 0$) we would achieve a triangular shape for the convolution in $A(\tau, \nu = 0)$. However, in Fig. 3 the ambiguity function is stretched in time domain due to the guard interval ($T_G > 0$), such that a flat plateau of length T_G is generated around $\tau = 0$. This stretching allows a time delay with a maximum spread $\tau_{max} \leq T_G$ resulting still in an orthogonal transmission under time-invariant multi-path fading. Nevertheless, by a small shift of the TF grid due to TO or CFO, the transmission will not be orthogonal anymore and many interference terms will appear in the TF grid.

In the first row of Fig. 4 the amplitudes of the effective channel matrix $|\mathbf{H}^{\mathsf{u}}|$ for OFDM ($T_G = 0$) and CP-OFDM ($T_G = 0.2T$) under different channel conditions for only one user u are depicted. Without TO and CFO, *i.e.* $\Delta\tau = 0$ and CFO $\Delta\nu = 0$, a pure diagonal structure for $|\mathbf{H}^{\mathsf{u}}|$ results for OFDM and CP-OFDM such that simple 1-tap equalization is sufficient. It can be observed that the structure of the effective channel matrix $|\mathbf{H}^{\mathsf{u}}|$ drastically changes in Fig. 4b for OFDM and Fig. 4c for CP-OFDM under exemplary offset conditions of CFO $\Delta\nu = 0.2F_0$ and TO $\Delta\tau = 0.2T$ leading to many off-diagonal elements. OFDM suffers from ISI and ICI caused by both offsets, whereas the CP-based scheme only suffers

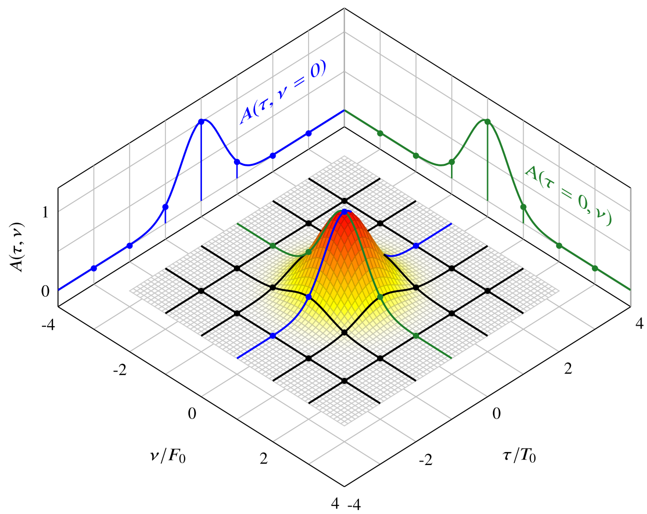

Fig. 5. Ambiguity function for Gaussian Tx/Rx filter with the localization parameter $\rho = 1$. The TF grid parameter is $F_0 = 1/T_0$.

from ICI due to the robustness against TO, while $T_G \geq \Delta\tau$. Nonetheless, with the presence of delay spreads larger than T_G or frequency shifts $\Delta\nu \neq 0$, the orthogonality is lost and a huge amount of interference will affect the transmission for OFDM and CP-OFDM.

2) Non-Orthogonal Transmission: FBMC schemes applying QAM mapping with general waveform, known as QAM/FBMC or sometimes generalized FDM (GFDM), are discussed in [44]–[47]. In contrast to CP-OFDM and OFDM, where the rectangular filter directly determines the TF grid, the application of general waveforms in QAM/FBMC offers a more flexible design in terms of TF grid density [15], [20]. The use of well-localized waveforms is more robust under practical constraints [20], [42], [44] and leads also to lower out-of-band (OoB) radiation. FBMC with *Gaussian waveform*

$$g(t) = (2\rho)^{\frac{1}{4}} \mathrm{e}^{-\pi\rho t^2} \tag{9}$$

with localization parameter $\rho \in [0, \infty)$ adjusting the shape in time and frequency domain and the *half-cosine waveform* (which is a special case of the root-raised cosine filter with roll-off-factor one)

$$g(t) = \frac{4\cos(2\pi t/T_0)}{\pi\left(1-(4t/T_0)^2\right)} \tag{10}$$

will always introduce interference terms on the adjacent TF grid points. Especially, a TF grid density close to $\delta_{\mathrm{TF}} = 1$ yields a non-orthogonal transmission [15], [20], but offers a higher spectral efficiency than CP-OFDM. For example, Fig. 5 shows the ambiguity function of the Gaussian waveform with localization parameter $\rho = 1$ leading to the same shape in time and frequency domain. It can be observed that each transmit signal has a considerable influence on the direct neighbors in the TF grid around the desired sampling point at $(0, 0)$. However, TF grid points of larger distance to the origin are almost unaffected in case of an offset shift of the TF grid.

The amplitudes of the effective channel matrix $\left|\mathbf{H}^{\mathsf{u}}\right|$ of the non-orthogonal schemes for one user are illustrated for the half-cosine waveform and the Gaussian waveform in the lower plots of Fig. 4. Without any offset ($\Delta\tau = 0$ and $\Delta\nu = 0$), the frequency-limited half-cosine offers an ICI-free transmission but suffers from ISI (see Fig. 4d). Contrarily, the well-localized Gaussian waveform introduces self-interference in both domains (ISI and ICI) as demonstrated in Fig. 4f. Both waveforms always inherently introduce interference terms, but the spread is mainly localized around the desired symbols. Even with TO and CFO the amplitude of the non-diagonal elements $\left|\mathbf{H}^{\mathsf{u}}\right|$ changes only marginally as shown exemplarily for $\Delta\tau = 0.2T$ and $\Delta\nu = 0.2F_0$ in Fig. 4e and Fig. 4g. This implies the robustness towards frequency and timing shifts and offers equalization techniques with marginally changing complexity at the receiver side.

C. OQAM-Based Schemes

In order to circumvent the drawback of QAM/FBMC that only waveforms with infinite shape yield an orthogonal transmission with a TF grid density $\delta_{\mathrm{TF}} = 1$, the combination of OQAM-based FBMC and so-called *TF staggering* can be used [43], [48]. Here, some well-localized and even-symmetric waveforms can achieve an orthogonal transmission with a critical-sampled TF grid. TF staggering stands for the use of two, but shifted, hexagonal TF grids yielding the overall TF grid depicted in Fig. 2b. One TF grid carries the real-valued symbol matrix $\mathrm{Re}\left\{\mathbf{D}^{\mathsf{u}}\right\}$ and the other TF grid the imaginary part $\mathrm{Im}\left\{\mathbf{D}^{\mathsf{u}}\right\}$, this is realized by the application of OQAM symbol mapping and the symbol phase parameter ϕ in Tab. I. One may note that the orthogonality condition changes from complex orthogonality (in orthogonal QAM-based schemes) to real-valued orthogonality [14], [42]. The OQAM-based FBMC transmission scheme achieves orthogonality only by applying the real part operator at the receiver after match filtering and equalization, *i.e.*, the interference part is purely imaginary. Both hexagonal TF grids have the same density ($\delta_{\mathrm{TF}} = 1$) but carry just "half a portion" of the symbols, leading to the same bandwidth efficiency as the QAM counterpart. However, only some filters allow an orthogonal transmission, *e.g.*, the rectangular waveform with an infinite shape in the frequency domain, the isotropic orthogonal transform algorithm (IOTA) [16], or the PHYDYAS filter [49]. The latter two filters offer a better spectral shape in comparison to the rectangular shape. In this work, we consider three OQAM-based schemes in Tab. I. Throughout this article, orthogonal OQAM-based schemes are called OQAM/OFDM (OQAM/OFDM), whereas non-orthogonal schemes are named OQAM/FBMC (OQAM/FBMC) achieving also a reduced amount of interference due to the TF staggering.

IV. Interference Analysis of FBMC in TWRC

We have seen in Fig. 4 that TOs and CFOs affect the effective channel matrix $\left|\mathbf{H}^{\mathsf{u}}\right|$ of the transmission schemes differently. The range of offsets in practical systems depends mainly on the technical precision of oscillators, the carrier frequency, the symbol rate, the relative velocity of the terminals and other issues like scattering and shadowing. Thus, to achieve comparable results, the subsequent analysis is done *w.r.t.* relative offsets normalized to the sub-carrier spacing F_0 and the core symbol length T of the rectangular filter. The impact of synchronization errors has been generally studied for OFDM beyond others in [50]–[52] and for general FBMC transmissions in [53]. Contrarily to P2P transmissions, the impacts of individual offsets in TWRC cannot be resolved individually at the relay [9], [11]. Even if the channel state information of both users are perfectly known, a complete compensation is impossible and, therefore, interference terms ② in (6) are not vanishing.

Subsequently, we will address the following questions: *How is the useful power of one symbol spread over the Rx-TF grid and is it sufficient to focus on a limited number of neighboring TF grid points?* The answer to this question is important for the design and the complexity of the FGE in Section V. Therefore, we analyze the influence of the introduced interference on the neighboring TF grid points at the relay with normalized signal power (*i.e.*, symbol variance $\sigma_{\mathrm{d}}^2 = 1$). Only one arbitrary but fixed symbol d_s^{u} per user at sending Tx-TF grid point (k, ℓ) with corresponding sending index $s = k + \ell N_{\mathrm{SC}}$ transmits to the relay. The useful power

$$P_{N_{\mathrm{N}}}^{\mathrm{QAM}} = \sum_{r \in \mathcal{D}_{\mathrm{N},s}^{\mathsf{A}}} \left| h_{r,s}^{\mathsf{A}} \right|^2 + \sum_{r \in \mathcal{D}_{\mathrm{N},s}^{\mathsf{B}}} \left| h_{r,s}^{\mathsf{B}} \right|^2 \tag{11}$$

considers the signal power at N_{N} Rx-TF-grid points for QAM-based schemes, where $\mathcal{D}_{\mathrm{N},s}^{\mathsf{u}}$ is a user-specific set of receive indices r according to the N_{N} largest amplitudes squared $\left| h_{r,s}^{\mathsf{u}} \right|^2$ for a given transmit index s. The OQAM-based FBMC transmission scheme achieves only orthogonality by applying the real part operator on the relay received signal $y_r^{\mathsf{R},\mathrm{OQAM}} = \mathrm{Re}\left\{ y_r^{\mathsf{R}} \right\}$ in (6) [54]. Hence, the useful power is defined as

$$P_{N_{\mathrm{N}}}^{\mathrm{OQAM}} = \sum_{r \in \mathcal{D}_{\mathrm{N},s}^{\mathsf{A}}} \mathrm{Re}\left\{ h_{r,s}^{\mathsf{A}} \right\}^2 + \sum_{r \in \mathcal{D}_{\mathrm{N},s}^{\mathsf{B}}} \mathrm{Re}\left\{ h_{r,s}^{\mathsf{B}} \right\}^2, \tag{12}$$

where the sets $\mathcal{D}_{\mathrm{N},s}^{\mathsf{u}}$ are generated according to the N_{N} largest real parts squared $\mathrm{Re}\{h_{r,s}^{\mathsf{u}}\}^2$. P_{Total} takes the overall available power at the relay into account. The set $\mathcal{D}_{\mathrm{N},s}^{\mathsf{u}}$ can be interpreted as the *neighborhood* of a symbol d_s^{u} with N_{N} neighbors. We further define the normalized power loss in logarithmic scale as

$$\gamma\left(N_{\mathrm{N}}\right) = 10 \log_{10}\left(\frac{P_{\mathrm{Total}} - P_{N_{\mathrm{N}}}}{P_{\mathrm{Total}}} \right), \tag{13}$$

giving the amount of signal power ignored by considering only N_{N} samples.

For the analysis of the seven different FBMC schemes in Tab. I, we assume a TWRC model with channel coefficients $h_{r,s}^{\mathsf{u}}$ given by (4). A TO $\Delta\tau^{\mathsf{u}}$ and a CFO $\Delta\nu^{\mathsf{u}}$ are present in the user-specific channels. We focus on symmetric compensation of all effects and, thus, an average compensation [11] is applied yielding $\Delta\tau^{\mathsf{B}} = -\Delta\tau^{\mathsf{A}}$ for the TO and $\Delta\nu^{\mathsf{B}} = -\Delta\nu^{\mathsf{A}}$ for the CFO, and a symmetric phase difference ϕ^{AB}.

Fig. 6 shows the normalized loss $\gamma\left(N_{\mathrm{N}}\right)$ for an increasing number of neighbors $N_{\mathrm{N}} = 1, 4, 7, 10, 13$ of the seven FBMC transmission schemes for varying TO $\Delta\tau^{\mathsf{u}}$, without phase shift ($\phi^{\mathsf{AB}} = 0$) and without CFOs ($\Delta\nu^{\mathsf{u}} = 0$). If no TO is present, *i.e.* $\Delta\tau^{\mathsf{u}} = 0$, the normalized power loss

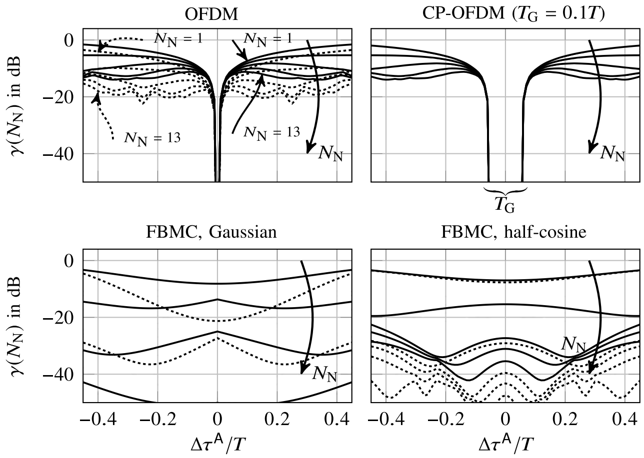

Fig. 6. Normalized loss for the QAM-based schemes (——) and OQAM-based schemes (..........) in Tab. I with $N_{\mathrm{N}} = 1, 4, 7, 10, 13$ considered neighbors applying TWRC, varying normalized TO $\Delta\tau^{\mathsf{A}}/T$, without CFO $\Delta\nu^{\mathsf{A}} = 0$ and without phase difference $\phi^{\mathsf{AB}} = 0$.

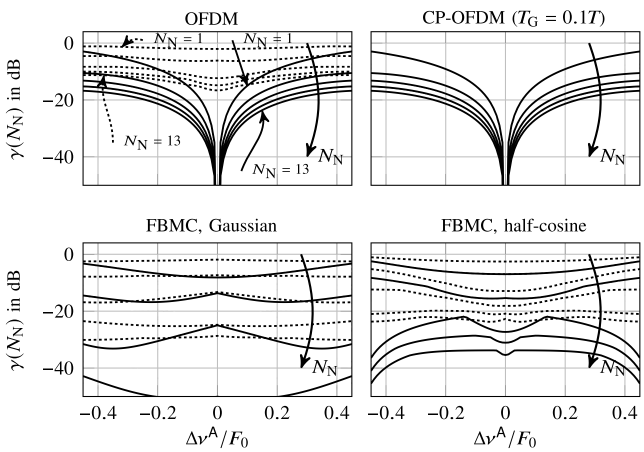

Fig. 7. Normalized loss for the QAM-based schemes (——) and OQAM-based schemes (..........), varying the normalized CFO $\Delta\nu^{\mathsf{A}}/F_0$, with phase difference $\phi^{\mathsf{AB}} = \pi/2$, $N_{\mathrm{N}} = 1, 4, 7, 10, 13$ without TO $\Delta\tau^{\mathsf{A}} = 0$.

$\gamma\left(N_{\mathrm{N}}\right)$ already vanishes for the orthogonal schemes if only one neighbor $N_{\mathrm{N}} = 1$ is considered. In contrast, for non-orthogonal FBMC all neighbors and, thus, the total power P_{Total} is required to achieve a completely vanishing power loss $\gamma\left(N_{\mathrm{N}}\right)$. As expected, the orthogonal CP-OFDM scheme does not suffer from a power loss as long as the TO is within the guard interval length T_{G}. In general, all schemes suffer from spreading over the TF grid with the presence of TO and the normalized loss $\gamma\left(N_{\mathrm{N}}\right)$ decreases by collecting more neighbors N_{N}. In the asynchronous case, the half-cosine and the Gaussian waveform require only a few neighbors N_{N} to achieve a lower loss over a wide range of offsets than the rectangular waveform in OFDM The OQAM-based schemes outperform the corresponding QAM schemes due to the better separation in the TF grid and the reduced interference power in the imaginary domain if no phase difference ϕ^{AB} occurs between the users.

Fig. 7 shows the normalized loss $\gamma\left(N_{\mathrm{N}}\right)$ for varying CFO $\Delta\nu^{\mathsf{u}}$ without a TO ($\Delta\tau^{\mathsf{u}} = 0$). Contrary to the setup in Fig. 6,

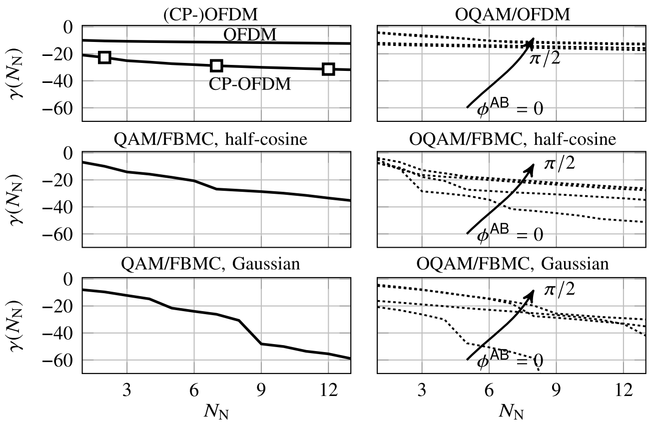

Fig. 8. Normalized loss applying TWRC with QAM-based (——) and OQAM-based (.........) FBMC schemes. Fixed TO $\Delta\tau^{A} = 0.05T$ and fixed CFO $\Delta\nu^{A} = 0.05F_0$. Varying $\phi^{AB} = 0, \frac{1}{9}\cdot\frac{\pi}{2}, \frac{5}{9}\cdot\frac{\pi}{2}, \pi/2$ over the number of neighbors N_N.

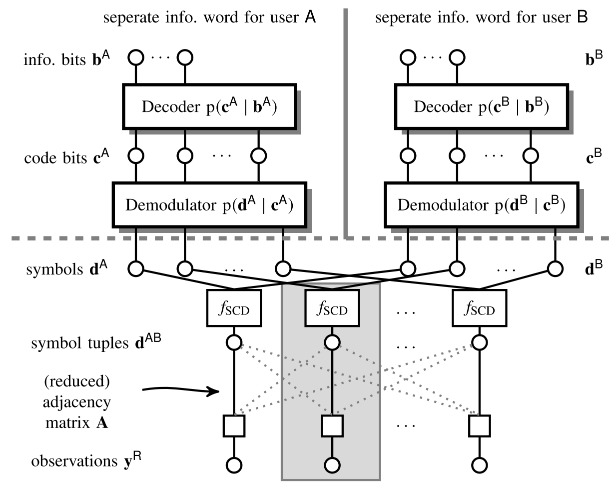

Fig. 9. SCD factor graph for the transmission of users A and B to the relay R. The part below the horizontal line consists of the equalizer part $p(\mathbf{y}^R \mid \mathbf{d}^u)$. The PLNC function f_{SCD} performs the tuple generation $\mathbf{d}^{AB} = \left(\mathbf{d}^A, \mathbf{d}^B\right)$ and marginalization.

a symmetric phase shift of $\phi^{AB} = \pi/2$ between the users is assumed. This phase shift destroys the real-valued orthogonality of OQAM/OFDM and the reduced interference of OQAM/FBMC (*i.e.* Re{②} ≫ 0). Correspondingly, a huge degradation in $\gamma(N_N)$ can be observed. Hence, the OQAM-based schemes introduce a high spread of the useful power in the TF grid. Although this scheme is orthogonal in a P2P transmission, in TWRC a high number of neighbors would be required (in the FGE in Section V) to collect the same amount of power as the QAM-based counterparts.

Finally, Fig. 8 indicates the behavior on the different FBMC schemes for a different number of neighbors N_N with varying phase shift ϕ^{AB} and fixed TO and CFO ($\Delta\tau^{A} = 0.05T$ and $\Delta\nu^{A} = 0.05F_0$). Generally, the more neighbors used, the lower the loss $\gamma(N_N)$. The lowest loss is achieved by the Gaussian waveform in both mapping schemes for a given $N_N > 1$ due to the good localization properties (also indicated by the ambiguity function in Fig. 5). It can further be observed that the QAM schemes are independent of the phase shift ϕ^{AB} leading to indistinguishable curves. In contrast, the OQAM schemes only achieve a low loss with phases shifts ϕ^{AB} close to zero. In contrast to P2P setups, the sensitivity to the unresolvable phase shifts in TWRCs concludes that OQAM-based schemes are not well suited with just one antenna at the relay. Thus, we focus on the QAM-based schemes for the further analysis, only. Nevertheless, we refer to [54] for a deeper analysis of OQAM/FBMC in a TWRC setup.

V. Detection and Decoding

In this section, we consider the three aforementioned PLNC detection/decoding schemes SCD, JCNC and G-JCNC to generate the BC message $\mathbf{b}^R$. In several publications [5], [7], [11], [41], it was shown that for the interference-free case, the three aforementioned schemes work well. However, the analysis in the previous section has shown that the famous CP-OFDM suffers severely under offset conditions and spreads the signal across a huge number of TF grid points at the relay. In contrast, the FBMC schemes applying well-localized waveforms used in QAM/FBMC introduce interference in a more "localized way" among a wide range of TO and CFO. In [1], we have proposed the use of an FGE, which is able to collect the useful signal along the TF grid points. Its complexity is mainly determined by the number of connections in the FG and it can be controlled by considering only the connections between observations and symbols with large channel coefficients $\left|h_{r,s}\right|$. Dependent on the PLNC approach, the FGE have to deliver different signal quantities to the detection/decoding entity. Furthermore, to improve the overall performance the output of the PLNC decoder is fed back to the FGE. Thus, the design of the FGE depends also on the PLNC approach, especially for the feedback message. To this end, we first introduce the FGE for SCD in detail *w.r.t.* the PLNC approach dependent implications. Afterward, we describe briefly the main difference concerning the schemes JCNC and G-JCNC.

A. Separate Channel Decoding (SCD)

The obvious approach is to estimate the information sequence $\mathbf{b}^u$ for each user separately based on the received signal $\mathbf{y}^R$ and perform the XOR combination $\mathbf{b}^R = \hat{\mathbf{b}}^A \oplus \hat{\mathbf{b}}^B$ based on the estimates $\hat{\mathbf{b}}^u$, afterward. In this work, the maximum a-posteriori (MAP) detection for each information bit b^u_ζ, $\zeta = 0, \ldots, N_b - 1$ given by

$$\hat{b}^u_\zeta = \arg\max_{b^u_\zeta \in \mathbb{F}_2} p(b^u_\zeta | \mathbf{y}^R) \tag{14}$$

is used. A powerful method to solve the marginalization needed in the MAP detection is given by the message passing *sum-product algorithm (SPA)* working on FGs. According to [23], the MAP detector (14) can be factorized into

$$\hat{b}^u_\zeta = \operatorname*{argmax}_{b^u_\zeta \in \mathbb{F}_2} \underbrace{p(\mathbf{y}^R|\mathbf{d}^u)}_{\text{Equalizer}} \underbrace{p(\mathbf{d}^u|\mathbf{c}^u)}_{\text{Demodulator}} \underbrace{p(\mathbf{c}^u|b^u_\zeta)}_{\text{Decoder}} \underbrace{\Pr\{b^u_\zeta\}}_{\text{a priori}}. \tag{15}$$

The corresponding FG for SCD is shown in Fig. 9. Each horizontal block corresponds to one part of the right-hand side of (15), where rectangular blocks indicate factor nodes and circles identify variable nodes. The exact implementation of the demodulation and decoder block is not in the scope of this paper. However, the application of LDPC codes are assumed with efficient FG implementations for decoding [55]. Due to the superposition of the symbols $\mathbf{d}^{\mathsf{A}}$ and $\mathbf{d}^{\mathsf{B}}$ in (3), the equalizer part in (15) can be further factorized to $\mathrm{p}(\mathbf{y}^{\mathsf{R}} \mid \mathbf{d}^{\mathsf{u}}) = \mathrm{p}(\mathbf{y}^{\mathsf{R}} \mid \mathbf{d}^{\mathsf{A}}, \mathbf{d}^{\mathsf{B}})\, \mathrm{p}(\mathbf{d}^{\mathsf{A}}, \mathbf{d}^{\mathsf{B}} \mid \mathbf{d}^{\mathsf{u}})$. The fully factorized FG is illustrated in the lower part of Fig. 9 (separated by the dashed line). The PDF $\mathrm{p}(\mathbf{y}^{\mathsf{R}} \mid \mathbf{d}^{\mathsf{A}}, \mathbf{d}^{\mathsf{B}})$ terms the relationship between the observation $\mathbf{y}^{\mathsf{R}}$ with the superimposed symbols $\mathbf{d}^{\mathsf{A}}$ and $\mathbf{d}^{\mathsf{B}}$. In addition, the PDF $\mathrm{p}(\mathbf{d}^{\mathsf{A}}, \mathbf{d}^{\mathsf{B}} \mid \mathbf{d}^{\mathsf{u}})$ connects the superimposed symbols with the user-specific symbols $\mathbf{d}^{\mathsf{u}}$ (illustrated as function node f_{SCD} in the FG).

1) Flexible Generation of the Factor Graph: The generation of the FG for the equalizer part $\mathrm{p}(\mathbf{y}^{\mathsf{R}} \mid \mathbf{d}^{\mathsf{A}}, \mathbf{d}^{\mathsf{B}})$ is the main focus of this work. In general, it can be described by the complete adjacency matrix $\mathbf{A}^{\text{complete},\mathsf{u}}$ [22], where each non-zero coefficient $h^{\mathsf{u}}_{r,s} \neq 0$ in the effective channel matrix $\mathbf{H}^{\mathsf{u}}$ leads to a coefficient $a^{\text{complete},\mathsf{u}}_{r,s} = 1$ in the adjacency matrix and thus to an edge in the FG connecting a variable node d^{u}_s with an observation node y^{R}_r.

We have seen in Section IV that well-localized waveforms spread their energy only to a limited number of neighbors in the TF grid at the relay. Therefore, we have used sets $\mathcal{D}^{\mathsf{u}}_{\mathrm{N},s}$ in (11) containing N_{N} indices of the elements with the highest impact on the transmission, indicated by the largest amplitudes squared $\left|h^{\mathsf{u}}_{r,s}\right|^2$. Based on these sets, we can now define a reduced adjacency matrix $\mathbf{A}^{\text{reduced},\mathsf{u}}$ determining only the *considered* edges within the FG for user $\mathsf{u} \in \{\mathsf{A}, \mathsf{B}\}$. The elements of the reduced adjacency matrix are then given by

$$a^{\text{reduced},\mathsf{u}}_{r,s} = \begin{cases} 1 & \text{if } r \in \mathcal{D}^{\mathsf{u}}_{\mathrm{N},s} \\ 0 & \text{otherwise} \end{cases}. \tag{16}$$

The complexity of the SPA working on the FG is mainly influenced by the number of edges [1]. The number of considered neighbors N_{N} is a trade-off parameter concerning the computational complexity and the accuracy of the algorithm later on. On the one hand, by setting $N_{\mathrm{N}} = N_{\mathrm{SC}} N_{\mathrm{TS}}$ (yielding the complete matrix $\mathbf{A}^{\text{complete},\mathsf{u}}$), even small amplitudes $\left|h^{\mathsf{u}}_{r,s}\right|$ lead to an edge in the FG. However, these connections will only have a small impact on the overall performance at the cost of a huge message exchange and calculation complexity. On the other hand, the choice of a too small number of considered neighbors N_{N} will produce only some connections within the FG, and thus, the complexity is reduced. However, with a high number of interference terms ② in (6), which are not considered in the FG, the accuracy of the FGE could be degraded. Based on the (reduced) adjacency matrix $\mathbf{A}^{\mathsf{u}}$ also a neighbor set $\mathcal{Y}_r$ for the observations can be defined as

$$\mathcal{Y}_r = \left\{ s \mid a^{\mathsf{A}}_{r,s} = 1 \vee a^{\mathsf{B}}_{r,s} = 1 \right\} \tag{17}$$

providing the neighborhood *w.r.t.* the observations y^{R}_r needed for the messages in the SPA.

2) SPA and Messages in the FG: The SPA is a formal description of exchanging messages on the edges between the variables and factor nodes. Illustratively, the message flow of the SCD detection scheme is shown for only one connection in the FG in Fig. 10, omitting the cross terms for simplicity. To simplify the notation, we introduce the PLNC factor node f_{SCD}, generating the symbol tuple $d^{\mathsf{AB}}_s = f_{\mathrm{SCD}}\big(d^{\mathsf{A}}_s, d^{\mathsf{B}}_s\big) = [d^{\mathsf{A}}_s \; d^{\mathsf{B}}_s]$ with cardinality M^2 for each sub-carrier kF_0 and time instance ℓT_0.

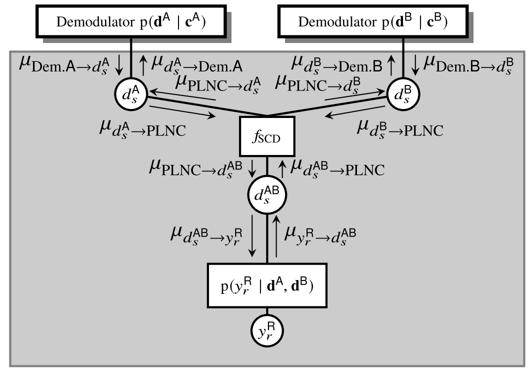

Fig. 10. Illustration of the messages flow for one edge in the gray part of the FG in Fig. 9. The cross terms are omitted for simplicity.

a) Message from observation node to symbol tuple node: The message between the observation factor node (connected to y^{R}_r) and the variable tuple node d^{AB}_s is calculated by

$$\mu_{y^{\mathsf{R}}_r\to d^{\mathsf{AB}}_s}\Big(d^{\mathsf{AB}}_s\Big) = \sum_{\sim\{d^{\mathsf{AB}}_s\}} \mathrm{p}(y^{\mathsf{R}}_r \mid \mathbf{d}^{\mathsf{A}}, \mathbf{d}^{\mathsf{B}}) \prod_{i\in\mathcal{Y}_r\setminus\{s\}} \mu_{d^{\mathsf{AB}}_i\to y^{\mathsf{R}}_r}\Big(d^{\mathsf{AB}}_i\Big) \tag{18}$$

where the term $\sum_{\sim\{d^{\mathsf{AB}}_s\}}$ is a shorthand notation for summing over all elements and realizations except the fixed realization d^{AB}_s connected in the FG to this node given by the adjacency matrix [23]. The message (18) performs the marginalization over the likelihood function

$$\mathrm{p}(y^{\mathsf{R}}_r \mid \mathbf{d}^{\mathsf{A}}, \mathbf{d}^{\mathsf{B}}) \propto \exp\left(-\frac{1}{\tilde{\sigma}^2_{\mathrm{n},r}} \left| y_r - \sum_{s\in\mathcal{Y}_r} h^{\mathsf{A}}_{r,s} d^{\mathsf{A}}_s - \sum_{s\in\mathcal{Y}_r} h^{\mathsf{B}}_{r,s} d^{\mathsf{B}}_s \right|^2 \right). \tag{19}$$

The noise term $\tilde{\sigma}^2_{\mathrm{n},r} = \sigma^2_{\mathrm{n}} + \sigma^2_{\mathrm{I},r}$ combines the variance of the AWGN and the power of the residual interference ignored by generating the FG with the reduced adjacency matrix $\mathbf{A}^{\text{reduced},\mathsf{u}} \neq \mathbf{A}^{\text{complete},\mathsf{u}}$. The ignored connections are modeled as an i.i.d. complex random variable with Gaussian distribution $\mathcal{N}_c\left\{0, \sigma^2_{\mathrm{I},r}\right\}$. The interference variance at each observation y^{R}_r is estimated by

$$\sigma^2_{\mathrm{I},r} = \sum_{i\in\overline{\mathcal{Y}}_r} \sigma^2_{\mathrm{d}} \left|h^{\mathsf{A}}_{r,i}\right|^2 + \sigma^2_{\mathrm{d}} \left|h^{\mathsf{B}}_{r,i}\right|^2, \tag{20}$$

where the sum runs over all elements in the complement set $\overline{\mathcal{Y}}_r = \{1, \ldots, N_{\mathrm{SC}} N_{\mathrm{TS}}\} \setminus \mathcal{Y}_r$, *i.e.*, all coefficients which are not considered in the actual FG but with a non-vanishing channel coefficient $\left|h^{\mathsf{u}}_{r,s}\right| \neq 0$.

b) Message from symbol tuple node to observation node: The message from a variable tuple node d_s^{AB} to a factor node y_r^{R} is the product of all incoming messages connected to this variable node given by

$$\mu_{d_s^{\mathsf{AB}} \to y_r^{\mathsf{R}}}\left(d_s^{\mathsf{AB}}\right) = \mu_{\mathrm{PLNC} \to d_s^{\mathsf{AB}}}\left(d_s^{\mathsf{AB}}\right) \prod_{i \in \mathcal{D}_{\mathrm{N},s} \setminus \{r\}} \mu_{y_i^{\mathsf{R}} \to d_s^{\mathsf{AB}}}\left(d_s^{\mathsf{AB}}\right). \quad (21)$$

The current a priori message from the PLNC function node to the variable tuple node in (21) is generated by

$$\mu_{\mathrm{PLNC} \to d_s^{\mathsf{AB}}}\left(d_s^{\mathsf{AB}}\right) = \mu_{d_s^{\mathsf{A}} \to \mathrm{PLNC}}\left(d_s^{\mathsf{A}}\right) \cdot \mu_{d_s^{\mathsf{B}} \to \mathrm{PLNC}}\left(d_s^{\mathsf{B}}\right). \quad (22)$$

The multiplication of the independent user-specific a priori messages coming back from PLNC detection/decoding part to the corresponding variable $\mu_{d_s^{\mathsf{u}} \to \mathrm{PLNC}}\left(d_s^{\mathsf{u}}\right)$ for all combinations *extends* the message space ($M \to M^2$).

c) Message from symbol tuple node to PLNC factor node: To generate the message of the variable tuple to the PLNC function f_{SCD}, all incoming messages are considered by

$$\mu_{d_s^{\mathsf{AB}} \to \mathrm{PLNC}}\left(d_s^{\mathsf{AB}}\right) = \prod_{i \in \mathcal{D}_{\mathrm{N},s}} \mu_{y_i^{\mathsf{R}} \to d_s^{\mathsf{AB}}}\left(d_s^{\mathsf{AB}}\right). \quad (23)$$

d) Message from PLNC factor node to the demodulator node: As mentioned before, the message on the right-hand-side in (23) contains the information of users A and B and, thus, it is of cardinality M^2. The message of a specific symbol d_s^{A} to the demodulator of user A is generated by the *marginalization* ($M^2 \to M$) of the corresponding symbols of user B by

$$\mu_{d_s^{\mathsf{A}} \to \mathrm{Dem.A}}(\mathcal{M}(\check{\mathbf{c}}^{\mathsf{A}} \overset{\mathrm{b2d}}{=} \kappa)) = \sum_{\check{\mathbf{c}}^{\mathsf{B}}} \mu_{d_s^{\mathsf{AB}} \to \mathrm{PLNC}}((\mathcal{M}(\check{\mathbf{c}}^{\mathsf{A}} \overset{\mathrm{b2d}}{=} \kappa), \mathcal{M}(\check{\mathbf{c}}^{\mathsf{B}}))), \quad (24)$$

treating the other user as interference. Here, the mapping $d_s^{\mathsf{A}} = \mathcal{M}(\check{\mathbf{c}}^{\mathsf{A}} \overset{\mathrm{b2d}}{=} \kappa)$ with "$\overset{\mathrm{b2d}}{=}$" is used as bijective mapping of a binary code vector $\check{\mathbf{c}}^{\mathsf{u}}$ containing $\log_2(M)$ pertinent code bits to the corresponding decimal index $\kappa = 0, \ldots, M-1$ out of M different symbols d_s^{A}. The message $\mu_{d_s^{\mathsf{B}} \to \mathrm{Dem.B}}$ for user B is calculated analogously.

e) Message passing: sum-product algorithm for the equalizer: The procedure of the SPA for the FGE is summarized in Alg. 1. The FG is initialized by the adjacency matrices $\mathbf{A}^{\mathsf{A}}$ and $\mathbf{A}^{\mathsf{B}}$ from (16). Usually this kind of FG has loops between neighboring variable tuples and factors nodes [35] and the solution (15) can only be found in an iterative way [23] in this case. Furthermore, the overall FG containing decoder, demodulator and equalizer is processed iteratively. If the demodulator stage provides a priori information based on the upper part of the overall FG, these messages are initialized as in line 5 of Alg. 1. However, if no a priori information is available (*e.g.*, in the first iteration) the messages are initialized as equally distributed (line 7 in Alg. 1). After some iterations, the messages are fed to the demodulator and the decoder detects the user-specific information words $\hat{\mathbf{b}}^{\mathsf{A}}$ and $\hat{\mathbf{b}}^{\mathsf{B}}$. Finally, the relay message is generated and transmitted in the BC phase.

Algorithm 1 FG-Based Equalizer: The SPA

1: ***#Initialize factor graph and messages#***
2: setup the edges based on the neighbor sets $\mathcal{D}_{\mathrm{N},s}^{\mathsf{u}}$ and $\mathcal{Y}_r$
3: $\mu_{y_r^{\mathsf{R}} \to d_s^{\mathsf{AB}}}\left(d_s^{\mathsf{AB}}\right) = 1/M^2$
4: **if** a priori information is available **then**
5: $\quad \mu_{d_s^{\mathsf{u}} \to \mathrm{PLNC}}\left(d_s^{\mathsf{u}}\right) = \mu_{\mathrm{Dem.u} \to \mathrm{PLNC}}\left(d_s^{\mathsf{u}}\right)$
6: **else**
7: $\quad \mu_{d_s^{\mathsf{u}} \to \mathrm{PLNC}}\left(d_s^{\mathsf{u}}\right) = 1/M$
8: **end if**
9: **repeat**
10: ***#Calculate variable to factor message#***
11: **for** $s = 0, s \le N_{\mathrm{SC}} N_{\mathrm{TS}} - 1, s = s + 1$ **do**
12: calculate $\mu_{d_s^{\mathsf{AB}} \to y_r^{\mathsf{R}}}\left(d_s^{\mathsf{AB}}\right)$ like in (21)
13: **end for**
14: ***#Calculate factor to variable message#***
15: **for** $r = 0, r \le N_{\mathrm{SC}} N_{\mathrm{TS}} - 1, r = r + 1$ **do**
16: calculate $\mu_{y_r^{\mathsf{R}} \to d_s^{\mathsf{AB}}}\left(d_s^{\mathsf{AB}}\right)$ like in (18) and (19)
17: **end for**
18: **until** Any stopping criterion is met
19: ***#Calculate equalizer output message#***
20: calculate $\mu_{d_s^{\mathsf{AB}} \to \mathrm{PLNC}}\left(d_s^{\mathsf{AB}}\right)$ (23) and $\mu_{\mathrm{PLNC} \to d_s^{\mathsf{u}}}\left(d_s^{\mathsf{u}}\right)$ (24)

B. Joint Channel Decoding and Physical-Layer Network Coding (JCNC)

As a matter of fact, the aim of the relay is to generate one mutual message for the BC phase. Thus, it is not interested in the individual messages, but in the joint PLNC message $\hat{\mathbf{b}}^{\mathsf{A} \oplus \mathsf{B}}$. By directly estimating the relay bit $\hat{b}_\zeta^{\mathsf{A} \oplus \mathsf{B}} = b_\zeta^{\mathsf{A}} \oplus b_\zeta^{\mathsf{B}}$ the MAP detector in (14) changes to

$$\hat{b}_\zeta^{\mathsf{A} \oplus \mathsf{B}} = \underset{b_\zeta^{\mathsf{A} \oplus \mathsf{B}} \in \mathbb{F}_2}{\mathrm{argmax}}\, \mathrm{p}(b_\zeta^{\mathsf{A} \oplus \mathsf{B}} | \mathbf{y}^{\mathsf{R}}). \quad (25)$$

The corresponding FG of the JCNC scheme is illustrated in Fig. 11 and applies only one chain *w.r.t.* the relay information word with just one demodulator estimating the XOR codeword $\mathbf{c}^{\mathsf{A} \oplus \mathsf{B}} \in \mathbb{F}_2^{N_c}$ and one binary decoder estimating $\hat{\mathbf{b}}^{\mathsf{A} \oplus \mathsf{B}} \in \mathbb{F}_2^{N_b}$. The equalizer for JCNC differs in the PLNC factor node f_{JCNC} (related to the factorization $\mathrm{p}(\mathbf{d}^{\mathsf{A}}, \mathbf{d}^{\mathsf{B}} \mid \mathbf{d}^{\mathsf{A} \oplus \mathsf{B}})$ similar to (15) for SCD), which maps the symbol tuple d_s^{AB} to one combined symbol $d_s^{\mathsf{A} \oplus \mathsf{B}}$ corresponding to the XORed combination of the underlying code bits. This mapping is necessary to enable a joint demodulator and decoder. The message from the PLNC block to the combined symbol $d_s^{\mathsf{A} \oplus \mathsf{B}}$ is calculated by the *marginalization* (*i.e.* changing the dimension from $M^2 \to M$) over the XORed combined bits given by

$$\mu_{\mathrm{PLNC} \to d_s^{\mathsf{A} \oplus \mathsf{B}}}(\mathcal{M}(\check{\mathbf{c}}^{\mathsf{A} \oplus \mathsf{B}} \overset{\mathrm{b2d}}{=} \kappa)) = \sum_{\check{\mathbf{c}}^{\mathsf{A}} \oplus \check{\mathbf{c}}^{\mathsf{B}} \overset{\mathrm{b2d}}{=} \kappa} \mu_{d_s^{\mathsf{AB}} \to \mathrm{PLNC}}((\mathcal{M}(\check{\mathbf{c}}^{\mathsf{A}}), \mathcal{M}(\check{\mathbf{c}}^{\mathsf{B}}))), \quad (26)$$

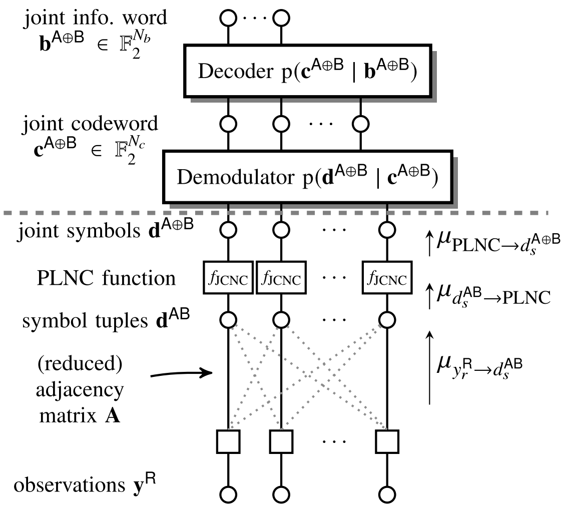

Fig. 11. FG used in the JCNC scheme with PLNC function node f_{JCNC} the symbol tuple d_s^{AB} to a joint symbol $d_s^{\mathsf{A}\oplus\mathsf{B}}$, and vice versa.

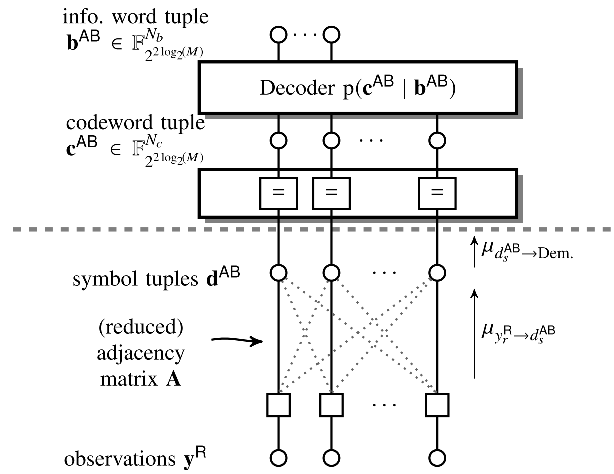

Fig. 12. FG for G-JCNC with decoder in Galois Field $\mathbb{F}_{2^{2\log_2(M)}}$ with direct message flow without marginalization.

where $\mu_{d_s^{\mathsf{AB}}\to\mathrm{PLNC}}$ is calculated by (23) and the index κ is the decimal representation regarding the XORed version of $\check{\mathbf{c}}^{\mathsf{A}} \oplus \check{\mathbf{c}}^{\mathsf{B}} \overset{\mathrm{b2d}}{=} \kappa$ with $\kappa = 0, \ldots, M-1$. The main advantage of the JCNC design is the application of only one state-of-the-art demodulator and binary decoder at the relay, leading to a lower computational complexity in comparison to the SCD scheme by a factor of two. However, reducing the message space in the upper part of the FG to the combined symbol $d_s^{\mathsf{A}\oplus\mathsf{B}}$ leads to an ambiguous assignment of the a priori message coming back from the decoder to the equalizer at the PLNC block as no information of the user-specific signals available. Hence, we can only use the *ambiguous mapping* (*i.e.* changing the dimension from $M \to M^2$) by

$$\mu_{\mathrm{PLNC}\to d_s^{\mathsf{AB}}}((\mathcal{M}(\check{\mathbf{c}}^{\mathsf{A}}), \mathcal{M}(\check{\mathbf{c}}^{\mathsf{B}})))\Big|_{\check{\mathbf{c}}^{\mathsf{A}}\oplus\check{\mathbf{c}}^{\mathsf{B}}\overset{\mathrm{b2d}}{=}\kappa} = \frac{1}{M}\mu_{d_s^{\mathsf{A}\oplus\mathsf{B}}\to\mathrm{PLNC}}(\mathcal{M}(\check{\mathbf{c}}^{\mathsf{A}\oplus\mathsf{B}} \overset{\mathrm{b2d}}{=} \kappa)). \quad (27)$$

Due to the direct estimation of the relay info word $\hat{\mathbf{b}}^{\mathsf{A}\oplus\mathsf{B}}$ the BC symbols can be generated by $\mathbf{d}^{\mathsf{R}} = \mathcal{M}(\mathcal{C}(\hat{\mathbf{b}}^{\mathsf{A}\oplus\mathsf{B}}))$, directly.

C. Generalized-Joint Channel Decoding and Physical-Layer Network Coding (G-JCNC)

The G-JCNC detection and decoding scheme estimates the relay information word jointly by a non-binary decoder in Galois Field $\mathbb{F}_{2^{2\log_2(M)}}$, fully exploiting the available information. Therefore, a joint code tuple $c_t^{\mathsf{AB}} \in \mathbb{F}_{2^{2\log_2(M)}}$ and a joint information bit tuple $b_\zeta^{\mathsf{AB}} \in \mathbb{F}_{2^{2\log_2(M)}}$ are defined. By extending the overall detection scheme to the variable tuples, the MAP detector for G-JCNC becomes

$$\hat{b}_\zeta^{\mathsf{AB}} = \underset{b_\zeta^{\mathsf{AB}}\in\mathbb{F}_{2^{2\log_2(M)}}}{\mathrm{argmax}} \; \mathrm{p}(b_\zeta^{\mathsf{AB}} \mid \mathbf{y}^{\mathsf{R}}). \quad (28)$$

The message from the equalizer (23) can directly be used without any marginalization (indicated by the "=" function node in Fig. 12), *i.e.*, no PLNC block is required in the FG offering the full available information at the decoder input. The main difference of the G-JCNC scheme compared to the other schemes is that a decoder for extension fields is required [5], [7]. In contrast to the JCNC scheme, the decoder offers a full feedback message $\mu_{\mathrm{Dem.}\to d_s^{\mathsf{AB}}}=\mu_{c_t^{\mathsf{AB}}\to\mathrm{Dem.}}$, directly applicable in the FGE, and thus, no marginalization or extension of the message space is required. After estimating the information word tuple $\hat{\mathbf{b}}^{\mathsf{AB}}$, the relay message is generated.

VI. Performance Evaluation

In this part the QAM-based FBMC systems in Tab. I with binary phase shift keying (BPSK) or 4-QAM modulation are applied. For LDPC encoding, a code rate of 0.3 and regular check degree of three are considered and the PEG algorithm [55] is applied to generate the parity-check matrix. The number of iterations for the LDPC decoding is set to 20. The time-variant multi-path channel is generated by 50 Rayleigh fading coefficients for each user resulting in the effective channel coefficients in (4). The time delay spread τ and the Doppler shift ν are equally distributed within $[0, \tau_{\max}]$ and $[-\nu_{\max}, \nu_{\max}]$, respectively. The maximum delay spread is set to $\tau_{\max} = 0.2T$ and additional individual CFOs of $\Delta\nu^{\mathsf{A}} = 0.2F_0$ and $\Delta\nu^{\mathsf{B}} = -0.2F_0$ are applied. In total, $N_{\mathrm{SC}} = 32$ sub-carriers and $N_{\mathrm{TS}} = 20$ time symbols are used to generate a frame containing 640 data symbols. Thus, each effective channel matrix $\mathbf{H}^{\mathsf{u}}$ contains 640^2 elements. The number of considered neighbors in the FGE is fixed to $N_{\mathrm{N}} = 1$ and $N_{\mathrm{N}} = 3$ and the number of iterations within the equalizer is set to three [1].

One may note that applying $N_{\mathrm{N}} = 1$ yields the 1-tap frequency domain equalizer commonly used in CP-OFDM. This configuration is sufficient for a synchronous transmission as the effective channel matrix is purely diagonal. However, in case of asynchronous transmission, CP-OFDM requires a high order equalizer to handle the occurring interference as indicated in Fig. 4.

Fig. 13a, Fig. 13b, and Fig. 14a show the FER performance of the three different PLNC detection/decoding schemes at the relay for all considered FBMC schemes with BPSK

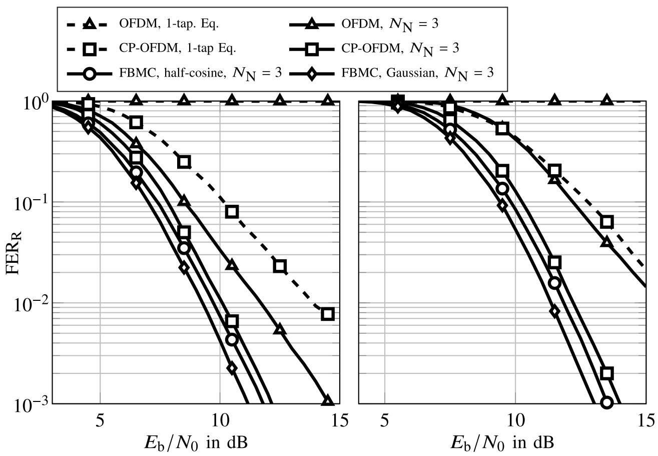

a) SCD, BPSK b) JCNC, BPSK

Fig. 13. FER performance at the relay applying the SCD and JCNC detector affected by max. delay spread $\tau_{\max} = 0.2T$ and CFOs $\Delta\nu^{\mathsf{A}} = 0.2F_0$ and $\Delta\nu^{\mathsf{B}} = -0.2F_0$ without Doppler shift $\nu^{\mathsf{u}} = 0$.

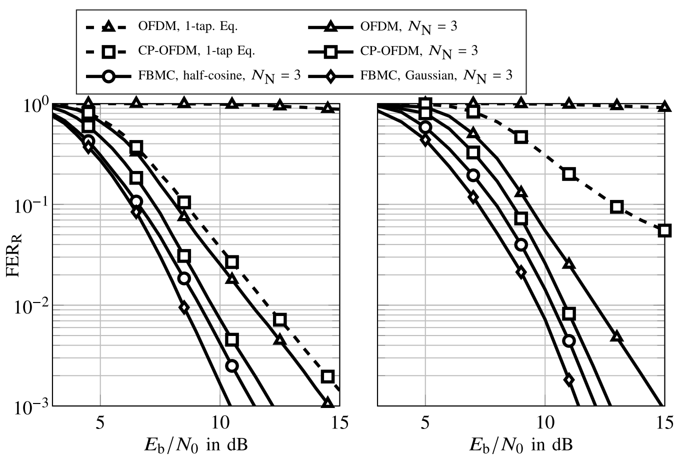

a) GJCNC, BPSK b) GJCNC, 4-QAM

Fig. 14. FER performance at the relay of the TWRC transmission applying the G-JCNC detector affected by max. delay spread $\tau_{\max} = 0.2T$ and CFOs $\Delta\nu^{\mathsf{A}} = 0.2F_0$ and $\Delta\nu^{\mathsf{B}} = -0.2F_0$ without Doppler shift $\nu^{\mathsf{u}} = 0$.

mapping. It can be observed for all PLNC approaches that the OFDM with 1-tap equalization suffers drastically from the additional interference introduced by the channel. As expected, OFDM is outperformed by CP-OFDM and a 1-tap equalizer ($N_N = 1$) due to the use of a CP. A significant gain is achieved in both schemes (OFDM and CP-OFDM) with the FGE and $N_N = 3$ neighbors. Applying general waveform in QAM/FBMC leads to an additional gain of roughly 1dB compared to the orthogonal schemes for all detection schemes at $\mathrm{FER} = 10^{-3}$ with the same computational complexity. Analyzing the FER performances *w.r.t.* the detection schemes show that the G-JCNC scheme outperforms all other schemes by the complete exploitation of the useful information from the equalizer to the demodulator in the FG. The SCD detection scheme performs slightly worse, as the marginalization over the users reduces the information in the FG. Both schemes outperform JCNC by roughly 2-3dB at $\mathrm{FER} = 10^{-3}$, due to the marginalization and the ambiguous feedback message from the demodulator. In Fig. 14b, we show the FER performance at

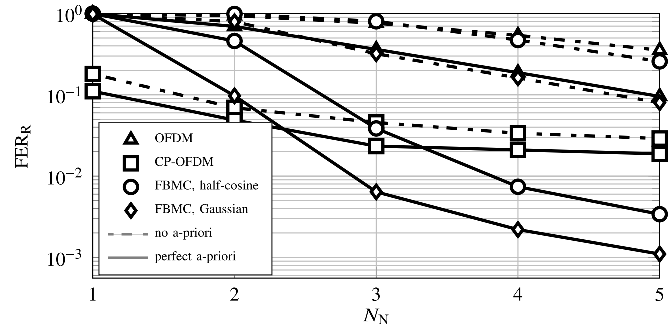

Fig. 15. FER performance at the relay at fixed SNR of 5dB and BPSK symbol mapping with different number of edges N_N in the FG applying the G-JCNC detector affected by time-variant channel ($\tau_{\max} = 0.2T$ and $\nu_{\max} = 0.2F_0$) with perfect and without a priori information in Alg. 1 lines 5 and 7, respectively.

the relay of G-JCNC applying BPSK and 4-QAM. The phase sensitivity of 4-QAM in TWRC [56] leads to a degradation of the performance of all transmission schemes. Especially, CP-OFDM with the simple 1-tap equalizer suffers drastically from this impact, whereas the performance with $N_N = 3$ neighbors shows only a minor loss for all schemes.

As the number of neighbors N_N determines the complexity, Fig. 15 shows the FER performance of the G-JCNC scheme for a varying number of considered edges $1 \leq N_N \leq 5$ per node in the FG with perfect a priori information (best-case scenario) and without a priori information (worst-case scenario) of the demodulator. The transmission is affected by a time-variant channel with $\tau_{\max} = 0.2T_0$ and $\nu_{\max} = 0.2F_0$ at a fixed SNR of 5dB. OFDM indicates only small improvements with a higher number of neighbors N_N. The CP-OFDM scheme starts with a lower FER at $N_N = 1$ due to the robustness introduced by the CP but also gains marginally by increasing $N_N > 1$. In contrast, FBMC starts with a high improvement utilizing only a few edges in the FG and the Gaussian waveform outperforms all other schemes for $N_N > 2$, due to the "well-localized" interference. All schemes suffer from unknown a priori information at the equalizer input and it can further be observed that a message exchange with the demodulator and decoder is essential at the relay. These FER characteristics coincide with the interference analysis versus the number of collected neighbors N_N in Fig. 8. All in all, the FER performance indicates the requirement of considering more neighbors in OFDM and CP-OFDM at the costs of higher complexity to achieve comparable results to the schemes with well-localized waveforms. The performance of the various combinations of transmission scheme and receiver approaches have been evaluated for a wide range of channel characteristics indicating advantages *w.r.t.* FER for OFDM/CP-OFDM in case of synchronous transmission and benefits for FBMC in case of asynchronous transmission under the assumption of same receiver complexity. However, FBMC offers better spectral efficiency and spectral shaping.

VII. CONCLUSION

This article provides a detailed overview of the impact of channel impairments like timing and frequency offsets, delay and Doppler spreads on the transmission within a two-phase TWRC. The interpretation of the transmission by FGs offers a deeper look into the structure by the effective channel matrix. The application of FBMC schemes with well-localized waveforms shows a significant reduction on the interference terms leading to only some adjacent cross connections in the FG, which offers the utilization of the FG-based equalizer at the relay. Three well-known PLNC detection/decoding schemes have been extended to work in combination with general FBMC schemes and FG-based equalization. We have further introduced the neighborhood parameter N_{N} within the algorithm to balance the complexity and accuracy of the algorithm. The FBMC schemes with well-localized waveforms outperform the well-known CP-OFDM even under severe channel conditions without the need for a CP and. Hence, they offer a higher spectral efficiency and further a lower OoB radiation. In the future, an adaptive system could offer the interaction between the relay and the users via a feedback link controlling, *e.g.*, the localization parameter ρ in the Gaussian waveform or the density δ_{TF} yielding a flexible control over the demand for the used spectrum, the required complexity for the equalizer and the FER performance at the relay.

References

[1] M. Woltering, D. Wübben, and A. Dekorsy, "Factor graph based equalizer for two way relaying channels with general waveforms," in *Proc. 20th Int. ITG Workshop Smart Antennas (WSA)*, Munich, Germany, Mar. 2016, pp. 1–8.

[2] S. Zhang, S. C. Liew, and P. P. Lam, "Hot topic: Physical-layer network coding," in *Proc. 12th Annu. Int. Conf. Mobile Comput. Netw. (ACM MobiCom)*, Los Angeles, CA, USA, Sep. 2006, pp. 358–365.

[3] P. Popovski and H. Yomo, "Physical network coding in two-way wireless relay channels," in *Proc. IEEE Int. Conf. Commun. (ICC)*, Glasgow, U.K., Jun. 2007, pp. 707–712.

[4] S. Zhang, S.-C. Liew, and P. P. Lam, "On the synchronization of physical-layer network coding," in *Proc. IEEE Inf. Theory Workshop (ITW)*, Chengdu, China, Oct. 2006, pp. 404–408.

[5] D. Wübben and Y. Lang, "Generalized sum-product algorithm for joint channel decoding and physical-layer network coding in two-way relay systems," in *Proc. IEEE Global Telecommun. Conf. (GLOBECOM)*, Miami, FL, USA, Dec. 2010, pp. 1–5.

[6] U. Bhat and T. M. Duman, "Decoding strategies at the relay with physical-layer network coding," *IEEE Trans. Wireless Commun.*, vol. 11, no. 12, pp. 4503–4513, Dec. 2012.

[7] D. Wübben, "Joint channel decoding and physical-layer network coding in two-way QPSK relay systems by a generalized sum-product algorithm," in *Proc. 7th Int. Symp. Wireless Commun. Syst. (ISWCS)*, York, U.K., Sep. 2010, pp. 576–580.

[8] S. C. Liew, L. Lu, and S. Zhang, *A Primer on Physical-Layer Network Coding*, vol. 8, J. Walrand, Ed. San Rafael, CA, USA: Morgan & Claypool, Jun. 2015.

[9] S. Zhang, S.-C. Liew, and H. Wang, "Synchronization analysis for wireless TWRC operated with physical-layer network coding," *Wireless Pers. Commun.*, vol. 68, no. 3, pp. 637–653, Feb. 2013.

[10] L. Lu, T. Wang, S. C. Liew, and S. Zhang, "Implementation of physical-layer network coding," *Phys. Commun.*, vol. 6, pp. 74–87, Mar. 2013.

[11] M. Wu, F. Ludwig, M. Woltering, D. Wübben, A. Dekorsy, and S. Paul, "Analysis and implementation for physical-layer network coding with carrier frequency offset," in *Proc. Int. ITG Workshop Smart Antennas (WSA)*, Erlangen, Germany, Mar. 2014, pp. 1–8.

[12] I. W.-H. Ho, S. C. Liew, and L. Lu, "Feasibility study of physical-layer network coding in 802.11p VANETs," in *Proc. IEEE Int. Symp. Inf. Theory (ISIT)*, Honolulu, HI, USA, Jun./Jul. 2014, pp. 646–650.

[13] G. Wunder *et al.*, "5GNOW: Non-orthogonal, asynchronous waveforms for future mobile applications," *IEEE Commun. Mag.*, vol. 52, no. 2, pp. 97–105, Feb. 2014.

[14] M. Bellanger, *FBMC Physical Layer: A Primer*, PHYDYAS FP7 Project Document, Jan. 2010. [Online]. Available: http://www.ict-phydyas.org/teamspace/internal-folder/FBMC-Primer_06-2010.pdf

[15] S. Schedler and V. Kühn, "Optimal lattice spacing for GFDM with Gaussian waveform," in *Proc. IEEE Wireless Commun. Netw. Conf. (WCNC)*, Doha, Qatar, Apr. 2016, pp. 1–6.

[16] B. Le Floch, M. Alard, and C. Berrou, "Coded orthogonal frequency division multiplex [TV broadcasting]," *Proc. IEEE*, vol. 83, no. 6, pp. 982–996, Jun. 1995.

[17] S. Schedler, M. Woltering, D. Wübben, V. Kühn, and A. Dekorsy, "Investigation on Gaussian waveforms to improve robustness in physical layer network coding," in *Proc. 18th Int. OFDM Workshop (InOWo)*, Essen, Germany, Aug. 2014, pp. 1–8.

[18] M. Woltering, D. Wübben, A. Dekorsy, S. Schedler, and V. Kühn, "Physical layer network coding using Gaussian waveforms: A link level performance analysis," in *Proc. 10th Int. ITG Conf. Syst., Commun. Coding (SCC)*, Hamburg, Germany, Feb. 2015, pp. 1–6.

[19] M. Woltering, D. Wübben, and A. Dekorsy, "Physical layer network coding with Gaussian waveforms using soft interference cancellation," in *Proc. IEEE 81th Veh. Technol. Conf. (VTC-Spring)*, Glasgow, U.K., May 2015, pp. 1–5.

[20] M. Woltering, S. Schedler, D. Wübben, A. Dekorsy, and V. Kühn, "Generalized multi-carrier waveforms in two-way relay systems," in *Communications in Interference Limited Networks*, W. Utschick, Ed. Berlin, Germany: Springer, Feb. 2016, pp. 475–499.

[21] F. R. Kschischang, B. J. Frey, and H.-A. Loeliger, "Factor graphs and the sum-product algorithm," *IEEE Trans. Inf. Theory*, vol. 47, no. 2, pp. 498–519, Feb. 2001.

[22] H.-A. Loeliger, "An introduction to factor graphs," *IEEE Signal Process. Mag.*, vol. 21, no. 1, pp. 28–41, Jan. 2004.

[23] H. Wymeersch, *Iterative Receiver Design*. Cambridge, U.K.: Cambridge Univ. Press, 2007.

[24] A. P. Worthen and W. E. Stark, "Unified design of iterative receivers using factor graphs," *IEEE Trans. Inf. Theory*, vol. 47, no. 2, pp. 843–849, Feb. 2001.

[25] G. Colavolpe and G. Germi, "On the application of factor graphs and the sum-product algorithm to ISI channels," *IEEE Trans. Commun.*, vol. 53, no. 5, pp. 818–825, May 2005.

[26] G. Colavolpe, "On LDPC codes over channels with memory," *IEEE Trans. Wireless Commun.*, vol. 5, no. 7, pp. 1757–1766, Jul. 2006.

[27] A. Anastasopoulos, K. M. Chugg, G. Colavolpe, G. Ferrari, and R. Raheli, "Iterative detection for channels with memory," *Proc. IEEE*, vol. 95, no. 6, pp. 1272–1294, Jun. 2007.

[28] Q. Guo and L. Ping, "LMMSE turbo equalization based on factor graphs," *IEEE J. Sel. Areas Commun.*, vol. 26, no. 2, pp. 311–319, Feb. 2008.

[29] R. J. Drost and A. C. Singer, "Factor-graph algorithms for equalization," *IEEE Trans. Signal Process.*, vol. 55, no. 5, pp. 2052–2065, May 2007.

[30] B. Y. Lu, G. Yue, X. Wang, and M. Madihian, "Factor-graph-based soft self-iterative equalizer for multipath channels," *EURASIP J. Wireless Commun. Netw.*, vol. 2005, no. 2, p. 687651, Apr. 2005. [Online]. Available: https://doi.org/10.1155/WCN.2005.187, doi: 10.1155/WCN.2005.187.

[31] M. N. Kaynak, T. M. Duman, and E. M. Kurtas, "Belief propagation over SISO/MIMO frequency selective fading channels," *IEEE Trans. Wireless Commun.*, vol. 6, no. 6, pp. 2001–2005, Jun. 2007.

[32] J. Hu and T. M. Duman, "Graph-based detection algorithms for layered space-time architectures," *IEEE J. Sel. Areas Commun.*, vol. 26, no. 2, pp. 269–280, Feb. 2008.

[33] P. Ochandiano, H. Wymeersch, M. Mendicute, L. Martínez, and I. Sobrón, "Factor graph based detection approach for high-mobility OFDM systems with large FFT modes," *EURASIP J. Wireless Commun. Netw.*, vol. 2012, no. 1, p. 331, Oct. 2012. [Online]. Available: https://doi.org/10.1186/1687-1499-2012-331, doi: 10.1186/1687-1499-2012-331.

[34] C.-W. Huang, P.-A. Ting, and C.-C. Huang, "A novel message passing based MIMO-OFDM data detector with a progressive parallel ICI canceller," *IEEE Trans. Wireless Commun.*, vol. 10, no. 4, pp. 1260–1268, Apr. 2011.

[35] X. Xu and R. Mathar, "Factor graph based detection and channel estimation for MIMO-OFDM systems in doubly selective channel," in *Proc. IEEE 7th Int. Symp. Wireless Commun. Syst. (ISWCS)*, Sep. 2010, pp. 456–460.

[36] L. Lu and S.-C. Liew, "Asynchronous physical-layer network coding," *IEEE Trans. Wireless Commun.*, vol. 11, no. 2, pp. 819–831, Feb. 2012.

[37] J. Huang, Z. Wang, S. Zhou, and Z. Wang, "Turbo equalization for OFDM modulated physical layer network coding," in *Proc. 12th Int. Workshop Signal Process. Adv. Wireless Commun. (SPAWC)*, Jun. 2011, pp. 291–295.

[38] Z. Wang, J. Huang, S. Zhou, and Z. Wang, "Iterative receiver processing for OFDM modulated physical-layer network coding in underwater acoustic channels," *IEEE Trans. Commun.*, vol. 61, no. 2, pp. 541–553, Feb. 2013.

[39] M. Hekrdla, "Design of modulations for wireless (physical-layer) network coding," Ph.D. dissertation, Elect. Eng. Inf. Technol., Czech Tech. Univ. Prague, Prague, Czech Republic, 2013.

[40] D. Wübben, M. Wu, and A. Dekorsy, "Physical-layer network coding with multiple-antenna relays," in *MIMO Processing for 4G and Beyond*, M. M. da Silva and F. A. Monteiro, Eds. Boca Raton, FL, USA: CRC Press, 2014, pp. 491–513.

[41] M. Wu, F. Ludwig, D. Wübben, A. Dekorsy, and S. Paul, "Physical layer cooperation in two-way relaying systems," in *Communications in Interference Limited Networks*, W. Utschick, Ed. Berlin, Germany: Springer, Feb. 2016, pp. 451–474.

[42] A. Şahin, I. Güvenç, and H. Arslan, "A survey on multicarrier communications: Prototype filters, lattice structures, and implementation aspects," *IEEE Commun. Surveys Tuts.*, vol. 16, no. 3, pp. 1312–1338, 3rd Quart., 2014.

[43] B. Saltzberg, "Performance of an efficient parallel data transmission system," *IEEE Trans. Commun. Technol.*, vol. COM-15, no. 6, pp. 805–811, Dec. 1967.

[44] W. Kozek and A. F. Molisch, "Nonorthogonal pulseshapes for multicarrier communications in doubly dispersive channels," *IEEE J. Sel. Areas Commun.*, vol. 16, no. 8, pp. 1579–1589, Oct. 1998.

[45] J. Du, "Pulse shape adaptation and channel estimation in Generalised frequency division multiplexing systems," Licentiate thesis, Electron. Comput. Syst., Royal Inst. Technol., Stockholm, Sweden, Nov. 2008.

[46] G. Fettweis, M. Krondorf, and S. Bittner, "GFDM—Generalized frequency division multiplexing," in *Proc. IEEE 69th Veh. Technol. Conf. (VTC-Spring)*, Barcelona, Spain, Apr. 2009, pp. 1–4.

[47] N. Michailow *et al.*, "Generalized frequency division multiplexing for 5th generation cellular networks," *IEEE Trans. Commun.*, vol. 62, no. 9, pp. 3045–3061, Sep. 2014.

[48] R. W. Chang, "Synthesis of band-limited orthogonal signals for multichannel data transmission," *Bell Syst. Tech. J.*, vol. 45, no. 10, pp. 1775–1796, Dec. 1966.

[49] A. Viholainen, T. Ihalainen, T. H. Stitz, M. Renfors, and M. Bellanger, "Prototype filter design for filter bank based multicarrier transmission," in *Proc. Eur. Signal Process. Conf. (Eusipco)*, Glasgow, U.K., Aug. 2009, pp. 1359–1363.

[50] M. Schellmann *et al.*, "FBMC-based air interface for 5G mobile: Challenges and proposed solutions," in *Proc. 9th Int. Conf. Cognit. Radio Oriented Wireless Netw. (ICST)*, Jun. 2014, pp. 102–107.

[51] T. Fusco, A. Petrella, and M. Tanda, "Sensitivity of multi-user filter-bank multicarrier systems to synchronization errors," in *Proc. IEEE 3rd Int. Symp. Commun., Control Signal Process.*, Mar. 2008, pp. 393–398.

[52] A. Aminjavaheri, A. Farhang, A. RezazadehReyhani, and B. Farhang-Boroujeny, "Impact of timing and frequency offsets on multicarrier waveform candidates for 5G," in *Proc. IEEE Signal Process. Signal Process. Edu. Workshop*, Aug. 2015, pp. 178–183.

[53] G. Matz, D. Schafhuber, K. Gröchenig, M. Hartmann, and F. Hlawatsch, "Analysis, optimization, and implementation of low-interference wireless multicarrier systems," *IEEE Trans. Wireless Commun.*, vol. 6, no. 5, pp. 1921–1930, May 2007.

[54] M. Woltering, M. Zhang, D. Wübben, and A. Dekorsy, "Comparison of general multi-carrier schemes in two way relaying channels," in *Proc. 20th Int. ITG Workshop Smart Antennas (WSA)*, Munich, Germany, Mar. 2016, pp. 1–6.

[55] X.-Y. Hu, E. Eleftheriou, and D. M. Arnold, "Regular and irregular progressive edge-growth tanner graphs," *IEEE Trans. Inf. Theory*, vol. 51, no. 1, pp. 386–398, Jan. 2005.

[56] M. Wu, D. Wübben, and A. Dekorsy, "Mutual information based analysis for physical-layer network coding with optimal phase control," in *Proc. 9th Int. ITG Conf. Syst., Commun. Coding (SCC)*, Munich, Germany, Jan. 2013, pp. 1–6.

Matthias Woltering (S'10) received the Dipl.-Ing. (FH) degree in electrical engineering from the University of Applied Science, Münster, Germany, in 2009, and the Dipl.-Ing. (Uni) degree in electrical engineering from the University of Bremen, Germany, in 2011, where he is currently pursuing the Ph.D. degree with the Department of Communications Engineering. Special research interests are wireless communications and signal processing in two-way relaying channels, especially in multi-carrier transmission schemes, detection, synchronization, and equalization techniques.

Dirk Wübben (S'01–M'06–SM'12) received the Dipl.-Ing. (FH) degree from the University of Applied Science, Münster, Germany, in 1998, and the Dipl.-Ing. (Uni) and Dr.-Ing. degrees from the University of Bremen, Germany, in 2000 and 2005, respectively, all in electrical engineering. In 2001, he joined the Department of Communications Engineering, University of Bremen, where he is currently a Senior Researcher and a Lecturer. His research interests include wireless communications, signal processing, cooperative communication systems, and channel coding.

Armin Dekorsy received the Dipl.-Ing. (FH) (B.Sc.) degree from Fachhochschule Konstanz, Germany, the Dipl.-Ing. (M.Sc.) degree from the University of Paderborn, Germany, and the Ph. D. degree from the University of Bremen, in communications engineering in 2007. He was a Research Engineer with Deutsche Telekom AG, and a Distinguished Member of Technical Staff with Bell Labs Europe, Lucent Technologies. In 2007, he joined Qualcomm GmbH as a European Research Coordinator, where he was involved in conducting Qualcomm's internal and external European research activities. He is currently the Head of the Department of Communications Engineering, University of Bremen, Germany. He has long term expertise in the research of wireless communication systems, baseband algorithms, and signal processing. He has authored over 160 journal and conference publications and holds over 17 patents in the area of wireless communications. He is a member of the IEEE Communications Society and the IEEE Signal Processing Society, the VDE/ITG Expert Committee on Information and System Theory, and represents the University at ETSI, NETWORLD2020, and the OneM2M forum.